Quantification of the Elastic and Relaxation Properties of Human Tunica Albuginea under Biaxial Loading

Sindy Hou

Thesis submitted to the Faculty of Virginia Polytechnic Institute and State University in partial fulfillment of the requirements for the degree of

Masters of Science
In
Engineering Mechanics

Vincent M. Wang, Chair
Raffaella De Vita
Sara L. Arena

July 10, 2019
Blacksburg, Virginia

Keywords: Biomechanics, Peyronie's Disease, Tunica albuginea, Biaxial, Digital Image Correlation, Stress Relaxation, Stiffness, Elastic Modulus

Quantification of the Elastic and Relaxation Properties of Human Tunica Albuginea under Biaxial Loading

Sindy Hou

Abstract

Peyronie's disease (PD) affects the tunica albuginea of the penis with a formation of dense and fibrous plaques. The plaques can cause a variety of symptoms in the patient such as pain during erection, erectile dysfunction, and penile disfigurement. There are many treatment options available, though none without disadvantages. Quantification of the material properties of the tunica tissue can inform potentially improved treatments. In this study tunica tissue (n=5) from donors were tested biaxially along the circumferential and longitudinal directions to a specified load magnitude and maintained at a fixed displacement for 30 minutes to allow for stress relaxation. The loading and relaxation were then repeated for a second time. Stiffness, Young's Modulus, strain at inflection point between the toe region and linear region on the stress-strain curve, as well as percent stress relaxation after 30 minutes were compared between anatomic directions and ramp number. Only stiffness and percent relaxation showed a statistically significant difference between ramps 1 and 2, regardless of direction ($p = 0.012$). The results from this study report the baseline data of the biaxial mechanical properties of the tunica albuginea to be used for future comparisons to the properties of PD and graft tissue.

Quantification of the Elastic and Relaxation Properties of Human Tunica Albuginea under Biaxial Loading

Sindy Hou

General Audience Abstract

Peyronie's disease (PD) affects a layer of tissue in the penis known as the tunica albuginea. Dense and fibrous plaques form on this layer which can cause pain during erection, erectile dysfunction, and penile disfigurement. There are many treatment options available, though none without disadvantages. In this study tunica tissues from donors were tested in order to find the material properties of the tissue to improve treatments. The tissue samples were pulled in tension in two directions simultaneously to a specified load magnitude and then held at a fixed displacement for 30 minutes. This protocol was then repeated a second time. The material properties of the tissue were compared between the anatomic directions of the tissue was well as protocol number. The results from this study report the baseline data of the biaxial mechanical properties of the tunica albuginea to be used for future comparisons to the properties of PD and graft tissue.

ACKNOWLEDGMENTS

I would like to thank my advisor, Dr. Vincent Wang, for his guidance, mentorship, and sponsorship over the last year.

I would like to thank Dr. Raffaella De Vita for her advice and direction whenever I needed it.

I would like to thank Dr. Judy Chun for instructing me with organ dissection.

I would like to thank Sabah Rezvani, Jeffrey McGuire, Alyssa Huntington, and my other coworkers for their support and friendship.

Table of Contents

List of Figures

List of Tables

1. Introduction

1.1. Clinical Background

Peyronie's disease (PD) is a disorder that affects the penis in the connective tissue in the tunica albuginea (TA) (Figure 1), which is mainly made of collagen and elastin [1]. Dense and fibrous plaques form at various sites within the TA, most commonly dorsally and laterally [2]. As the disease progresses, the plaques may ossify, creating extremely inelastic masses on an elastic tissue, which likely causes a variety of problematic symptoms for the patient. These can include pain during erection, erectile dysfunction (ED), penile curvature, deformity, narrowing, and hinging (a buckling effect due to a narrow segment of the shaft) [3]. The size of the plaque has shown no correlation to the severity of symptoms [4].

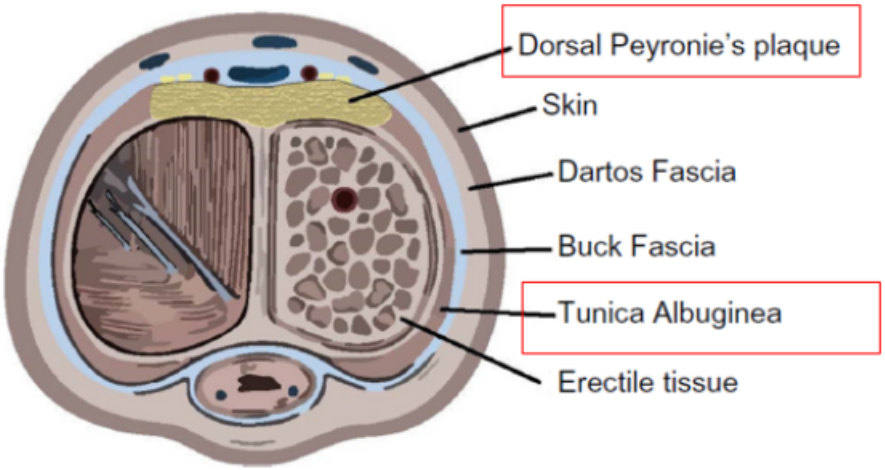

Figure 1: Cross-sectional view of penile anatomy and location of the TA [5].

During a normal erection in a healthy penis, a computational study [6] indicated that mechanical stresses are dispersed throughout the organ (Figure 2), allowing the nerve endings, blood vessels, and vascular bed to share equal local pressure. Though the plaques themselves are painless, their existence very likely cause the mechanical stresses to be redistributed along the organ (Figure 3), which can then increase the local pressure on nerve endings, which are sensitive to any changes in stress distribution. [2].

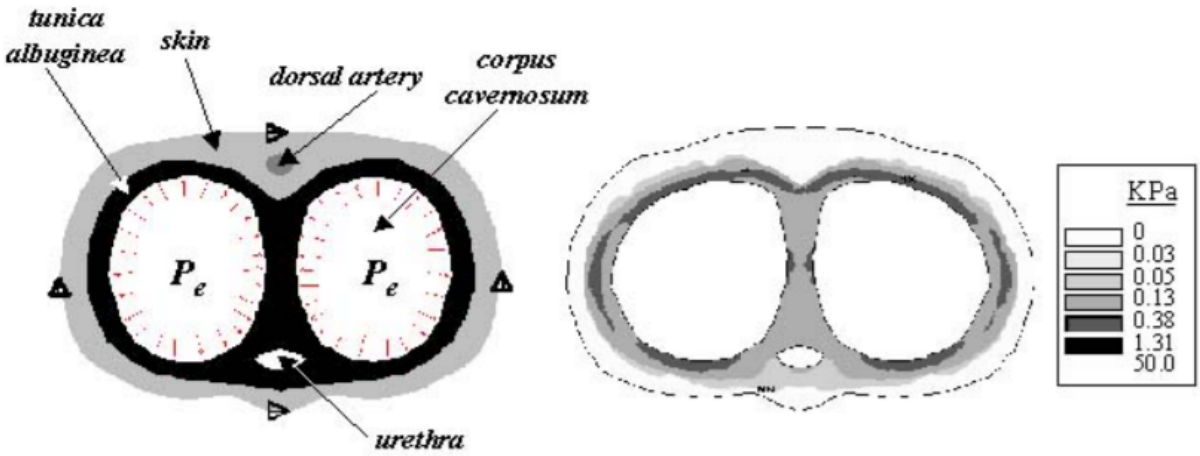

Figure 2: von Mises stress distribution in cross section of healthy penis model during full erection [6]

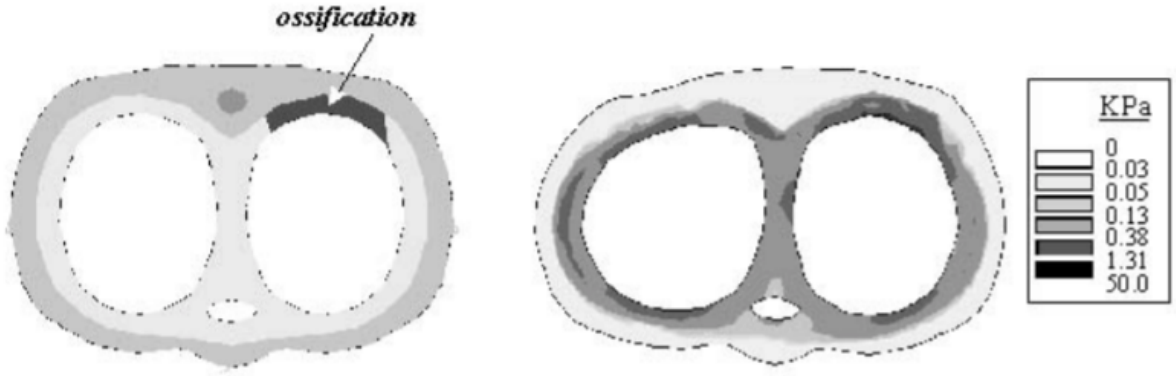

Figure 3: von Mises stresses in cross section of penis with Peyronie's plaque model during full erection [6]

Though PD can affect up to 13% of the male population, there is still no consensus on a definitive cause of the disease [7]. However, there are a few common factors that are thought to contribute to the development of this disease. PD prevalence is higher in cases where the patient is older (55 years, [8]), already has ED, diabetes, a smoking habit, or various cardiovascular diseases such as high blood pressure, heart insufficiency, and arteriosclerosis [9] [8].

The estimated percentage of affected males is likely underestimated considering the personal nature of the condition and those with PD could be reluctant to seek help. Those who do seek help are usually treated with the goals to reduce curvature and pain as well as restore penile function [10]. Within the first 12 months of disease onset, also known as the acute stage, there are non-surgical treatment options [4]. However, there can be a myriad of side effects with mixed results [10]. After the initial 12 months, and once the

disease has stabilized, also known as the chronic stage, surgical treatment is recommended [11].

There are multiple surgical treatment options for PD, the choice of which depends on the progression of the disease and the goals of the patient post treatment. Commonly, the options are tunical albuginea plication (TAP), plaque excision and grafting (PEG), or an inflatable penile prosthesis (IPP) [11]. Though the three all vary in their advantages and disadvantages, there is no significant difference in patient-described satisfaction postoperatively. TAP commonly results in penile shortening, so it is usually reserved for cases that are less than 60 degrees of curvature. IPP is usually given to those with an unsatisfactory rigidity in their erection. PEG is recommended for those with the most severe cases of PD such as a curvature of greater than 60 degrees, and/or a so-called hourglass deformity [12]. Though PEG has the highest reported patient satisfaction with penile rigidity (72.4%) improvements to the biocompatibility of the graft material could improve other post-operative outcomes such as ability to engage in sexual intercourse (83.3%) and residual curvature (18.4%) [11].

Penile traction therapy (PTT), a non-surgical mechanical intervention, can be implemented with a combination of traction and vacuum devices to treat PD. It has been shown to reduce curvature as well as plaque volume and additionally can increase penile length. A study showed that men can see a reduced curvature of 10-40 degrees, increased penile length of 1-2.5 cm and enhanced girth. No adverse effects were seen on the men in the study [13]. The penis is placed in a device that stretches it at a certain length for a prescribed amount of time. PTT involves a prolonged tension at a set displacement, thought there is currently debate on the device application (3 to 6 hours) and treatment duration (3 to 6 months) of PTT [14].

1.2. Tissue Biomechanics

It is assumed that PD plaques in the penis can alter the material properties of the TA by increasing the stiffness as the plaques [10]. There have been no experimental studies at this time that compare the diseased and healthy TA tissue on a biomechanical level. One previous study examined the elasticity and tensile strength of the TA, but only used slices of tissue (thickness of 1.3 to 3.3 mm) in a uniaxial tensiometer. This study reported an elastic modulus of approximately 100 MPa [15]. An additional study looked at the breaking point pressure (penetration stress) tension test of the TA tested in the most distal portion of dissected tissue [16]. The two studies focus on small regions of tissue rather than larger, and do not include the bi-directionality of the tissue. Since i*n vivo* the tissue behaves as a continuous surface as opposed to a single point or small section, the tissue needs to be tested in a way that replicates this.

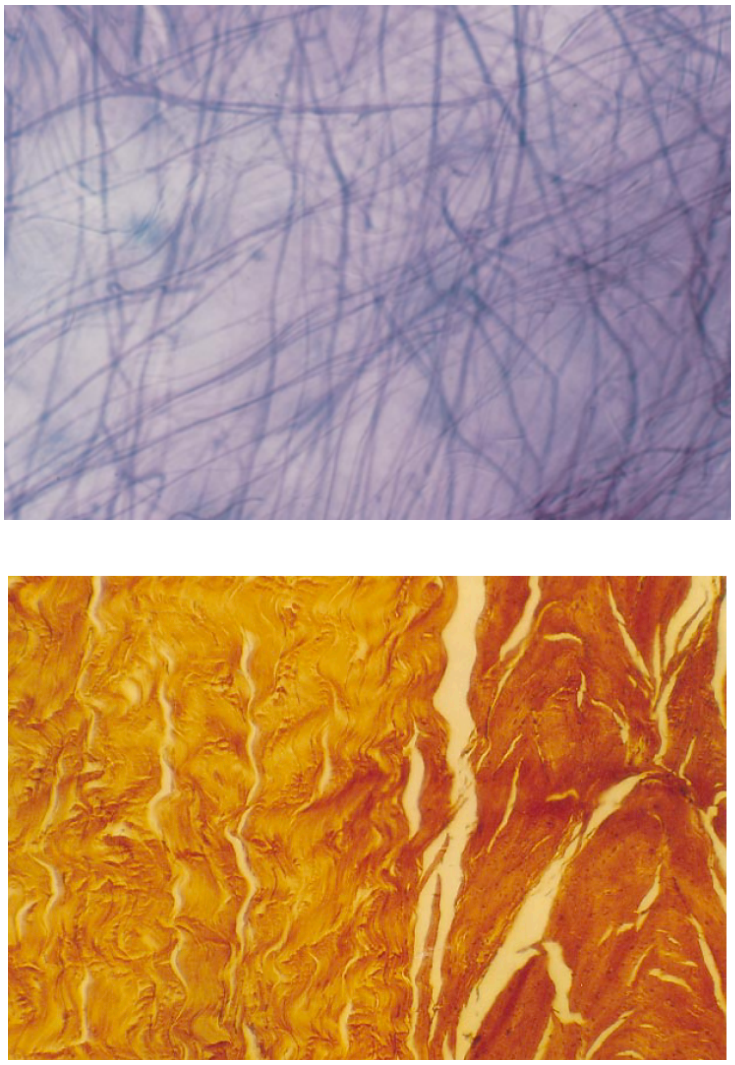

Figure 4: Top picture: Network of elastic fibers of regular size, length, and direction in non-diseased TA tissue (50 μm section, Hart's stain x100). Bottom picture: Undulating collagen fibers of similar size in non-diseased TA tissue (5 μm section, Hart's stain x100) [17].

In vivo during an erection the TA will experience tension in two directions, longitudinally and circumferentially (Figure 4). The collagen bundles and elastin fibers are arranged in the TA with the inner layer circumferential and the outer layer longitudinal. The elastin fibers form a lattice network that support the collagen bundles [17]. The complexity of the tissue matrix structure likely leads to mechanical anisotropy, and biaxial testing will allow for a more physiologically appropriate analysis [18].

The elasticity and viscoelasticity of the tissue needs to be quantified in order to characterize the material properties of the TA (Figure 5). With the application of

progressively increasing tension, stiffness and Young's Modulus of the TA can be quantified, which can be useful in the creation and selection of skin grafts for surgical reconstruction [12]. While characterizing the non-linear elastic behavior of collagenous tissues, there are three main regions on the stress strain curve: the toe region, linear region, and failure region. The toe region is the early loading phase, where the fibers in the tissue are un-crimping and the slope on the stress strain curve is low. After the majority of the fibers have been recruited (uncrimped), the linear region begins where the fibers actually stretch. The point of transition between the toe region and the linear region is the inflection point. After this region is the failure region, the point where the fibers are stretched to the point of breakage [19] (Figure 6). Additionally, viscoelasticity describes the time-dependent response of materials. One parameter for which viscoelasticity can be quantified is tress relaxation, where the stress is measured while maintaining a fixed magnitude of applied strain for a specified period of time.

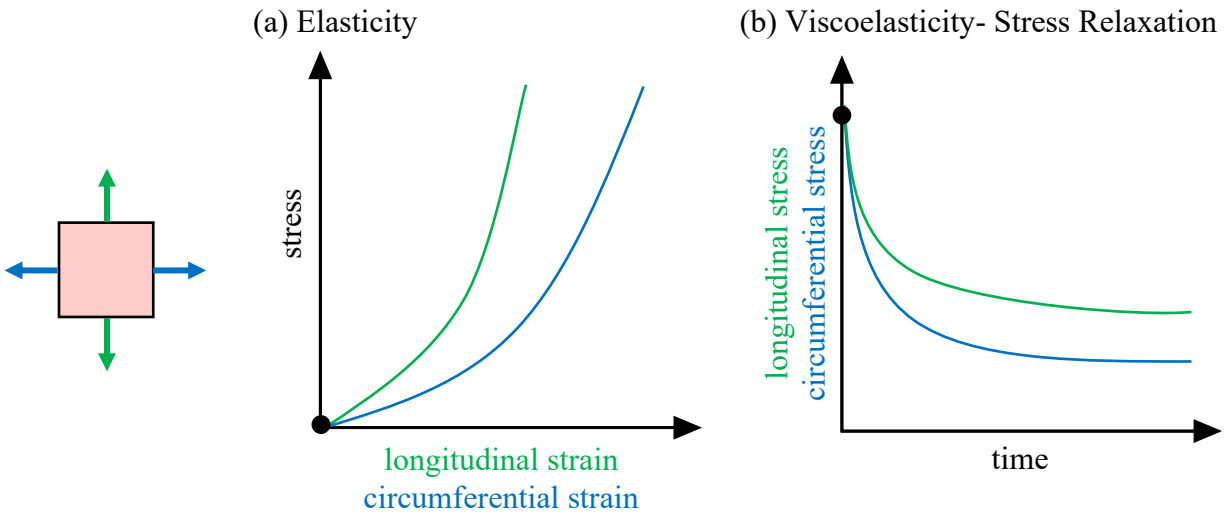

Figure 5: a: stress-strain graph, where the slope of the linear region is the elastic modulus b: stress-time graph where tissue strain is maintained for a specified duration of time, showing stress relaxation

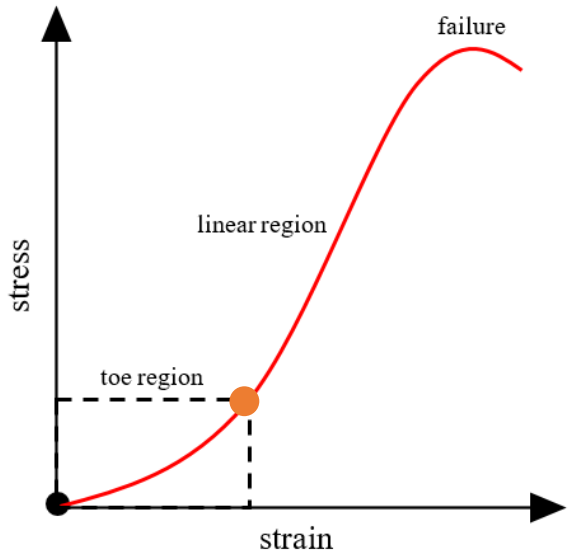

Figure 6: Representative stress-strain curve with defined toe region, linear region, and failure point. Orange circle represents the inflection point.

1.3. Digital Image Correlation

Digital image correlation (DIC) is a non-contact technique to optically measure strain and displacement. DIC uses a collection of grey-scale images taken at continuous timepoints of a deformation and tracks the movement of pixels in the region of interest. The software calculates strain and displacement fields using a correlation algorithm [20]. DIC has been extensively used with biological tissues such as cartilage, tendons, and soft tissue, including the uterosacral ligament as well as vaginal tissue, both uniaxially and biaxially [21-24]. Biological samples are extremely variable in regards to many physical properties so DIC is preferable to see the full strain field. A full field of measurement also allows a complete assessment of local change on an inhomogeneous sample [24].

1.4. Objective

To quantify the elastic and viscoelastic properties of non-diseased tunica albuginea tissue.

a) To compare material properties between the longitudinal and circumferential directions.
b) To compare the material properties between repeated loads to examine material changes after loading.

2. Methods

2.1. Specimen Preparation

Donor organs were collected from United Tissue Network (UTN) with a desired age range between 30 and 70 years, as well as exclusions for PD risk factors such as diabetes, smoking habits, and cardiovascular diseases. Organs were shipped frozen and immediately stored in a -20 º C freezer until ready for the day of testing, following IBC-approved protocols. The donors for the reported data used for this study are listed in Table 1.

Donor Identification Number	Age	Regions Dissected
GL1808774	49	Proximal
GL1810684	32	Proximal
GL1809101	42	Distal
GL1808895	58	Proximal and Distal

Table 1: Age and regions isolated from donors.

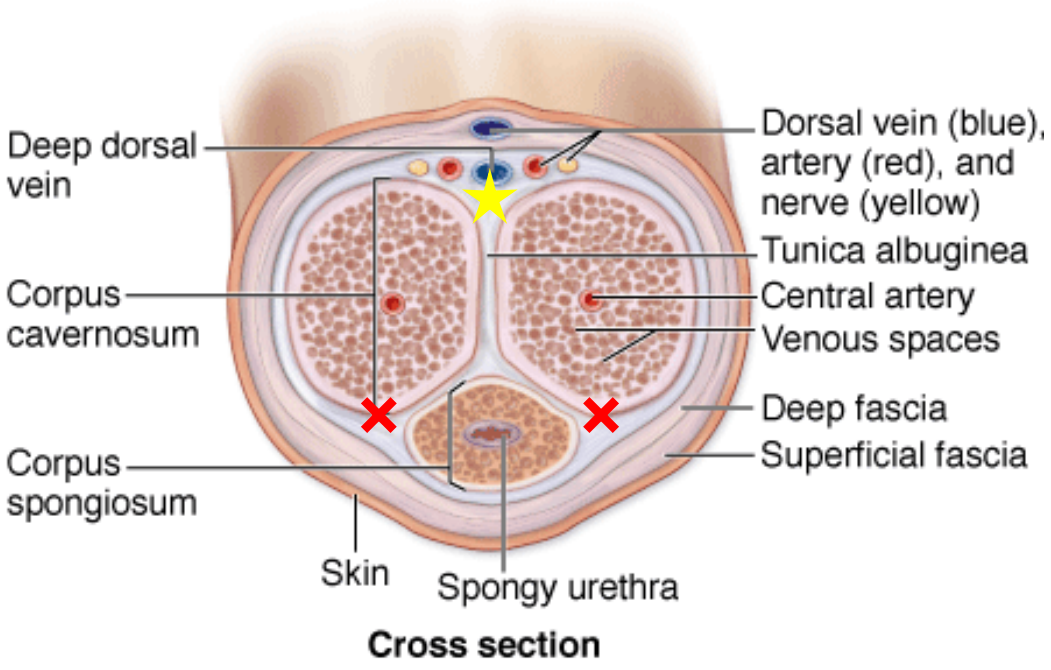

Figure 7: Schematic of the anatomy of the cross section and layers of the human penis [25].

Figure 8: Longitudinal cut into the corpus cavernosum after degloving in order to better visualize the TA for dissection.

Two days prior to testing the organ was removed from the freezer and was thawed and the next day was dissected. A continuous cut was made underneath the glands of the organ which was used to then fully "deglove" the specimen by removing the outer layer of skin (Figure 7). A rod like object was inserted into the ureter in order to isolate the urethra inside the corpus spongiosum, which was then dissected out as well. Once the glans was removed, two longitudinal cuts were made into each corpus cavernosa (Figure 8), starting at the marked x's in Figure b and terminating around the central artery. The corpus cavernosum is then removed from the tunica albuginea by separating the two layers with dissection scissors circumferentially and superiorly, until the two cuts meet at the fibrous septum, marked by the star in Figure 7. The fibers of the septum were then cut to obtain a flat sheet of TA tissue. The Bucks Fascia, remaining corpus as well as the dorsal arteries were then slowly dissected off to isolate the TA. This was then marked with a surgical pen in order to mark 3 cm by 3 cm squares with the septum as a midline. If the TA sheet was large enough, two samples: proximal (P) and distal (D) could be obtained (Figure 9), otherwise, only one sample was attained. These samples were then marked and wrapped in saline soaked gauze and placed in the refrigerator until the next day.

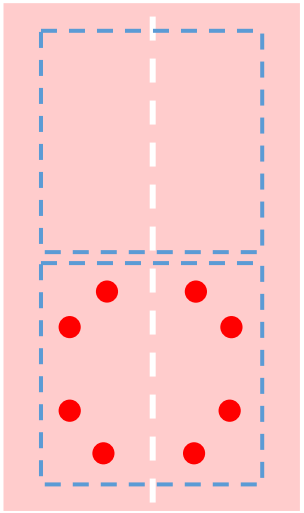

Figure 9: Representative diagram of large isolated TA tissue. 3 cm by 3 cm squares marked for further division. The septum (white dotted line) follows the longitudinal direction while perpendicular to that is the circumferential direction. The eight approximate locations of thickness measurement on the TA are marked with red dots.

The thickness of each sample was measured at eight locations (Figure 9) of the sample with a laser displacement sensor (Keyence, LK G82, Itasca, IL) (Table 2). The samples were then placed in a petri dish with 1X Phosphate Buffered Solutions (PBS, Fisher Science Education, USA) for 15 minutes and the thickness was repeated and these measurements were averaged. After the samples were hooked onto the biaxial machine, the dimensions of the testing field (Figure 11) were 2.5 cm by 2.5 cm, which was multiplied by the average thickness to estimate the cross sectional area [26]. For a particular specimen, measured forces were normalized to its computed CSA in order to compute stress.

Sample Identification	Median Thickness (mm)
101D	3.285 ± 0.672
684P	2.841 ± 0.503
774P	3.352 ± 0.954
895D	2.905 ± 0.803
895P	3.998 ± 0.674

Table 2: Average thickness of samples in millimeters.

2.2. Mechanical Testing

Methylene Blue (Fisher Science Education, USA) was then added into the petri dish with PBS and the samples were soaked for an additional 15 minutes to allow the dye to completely saturate for a sufficient contrast against a contrasting pattern. After soaking, the sample was sandwiched between two custom 3D printed grid stencils in order to puncture through with pairs of safety pins connected with a length of nylon wire. The samples were then speckled with white spray paint in order to make a sufficient pattern for the DIC, about 50% speckle density (Figure 10) (VIC-3D, Correlated Solutions, SC) [26].

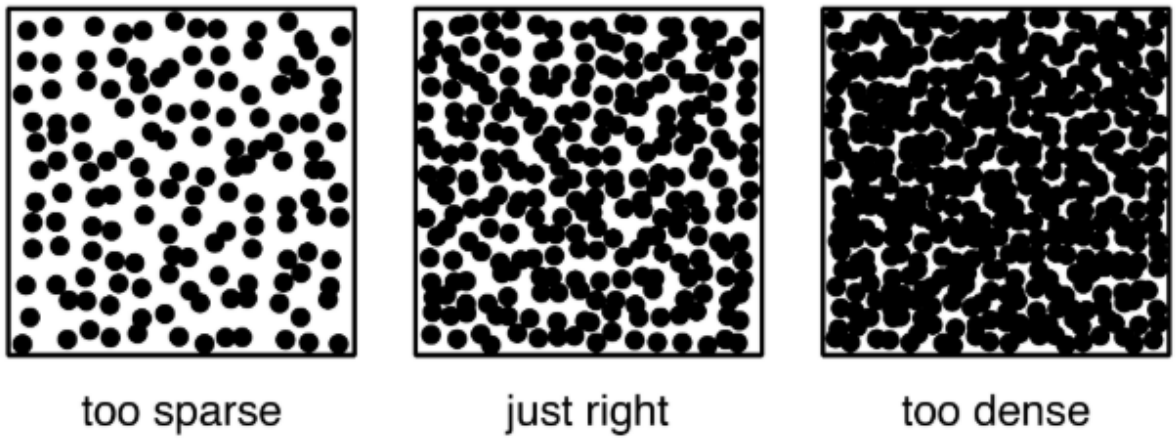

Figure 10: DIC speckle pattern standards to use for comparison and confirmation of sufficient speckling [27].

The sample was then loaded onto the biaxial instrument with the septum designated the longitudinal direction while perpendicular to the septum was designated the circumferential direction, and allowed to rest in the PBS in order for the dye to dilute (Figure 11). The sample was preconditioned to 5% of the initial length at a rate of 0.1mm/s for 50 cycles until a consistent load-displacement graph was achieved. After preconditioning, samples were then subjected to the following testing sequence: (1) loading of sample at a rate of 0.1 mm / s until the measured load in each direction reached 45N, (2) displacement held for 30 minutes to allow the tissue to undergo stress relaxation, (3) unloading at a rate of 0.1 mm / s until both directions of the load cells reached 0.5 N. The load was then manually lowered to around 0.2 N in both directions and the tissue allowed to recover for 2 hours in the PBS, while ensuring that the sample was under minimal loading. Steps 1-3 were designated as “Ramp 1”. The testing sequence was then repeated a second time which was designated “Ramp 2”. Images were recorded at a rate of 2 Hz while the biaxial load and displacement data were collected at a

rate of 10 Hz. Since the two sets of data were taken at different rates, they were then manually synchronized.

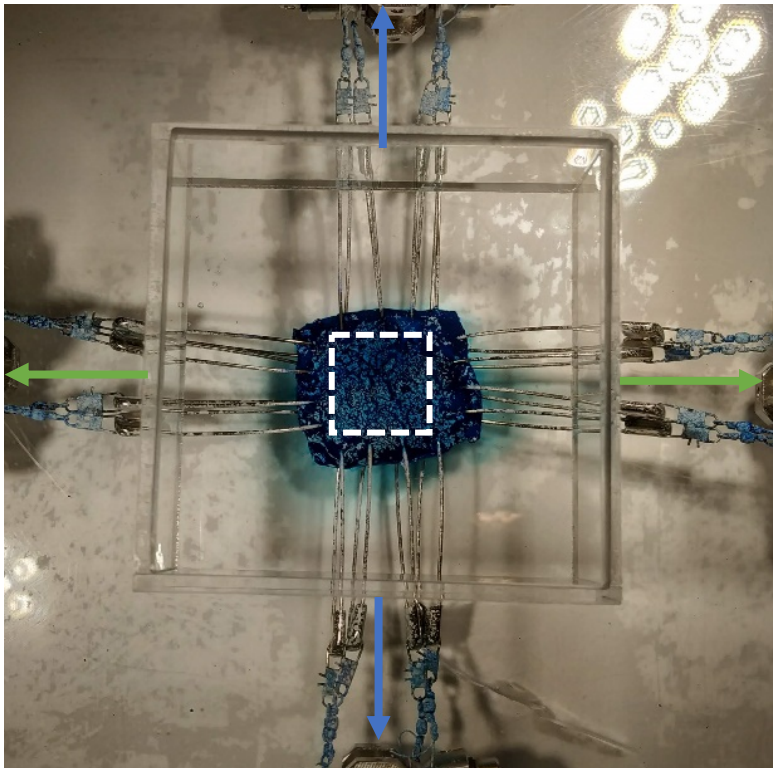

Figure 11: TA tissue pinned and speckled with high-contrast paint for DIC analysis during biaxial load testing. Green arrows represent the longitudinal direction, blue arrows represent the circumferential direction. White dashed line represents the approximate 2.5 by 2.5 cm testing field.

2.3. Data Analysis

DIC images were processed in the VIC-3D software after assigning an x and y axis of analysis with x being longitudinally along the septum and y being circumferentially. These images were then analyzed in order to calculate the normal and shear strain from the Green Strain tensor (Eqs. 1-3) [28].

$$\boldsymbol{E} = \begin{bmatrix} Exx & Exy & Exz \\ Exy & Eyy & Eyz \\ Exz & Eyz & Ezz \end{bmatrix} \tag{1}$$

$$E_{xx} = \frac{\partial u}{\partial x} + \frac{1}{2}\left[\left(\frac{\partial u}{\partial x}\right)^2 + \left(\frac{\partial v}{\partial x}\right)^2 + \left(\frac{\partial w}{\partial x}\right)^2\right] \tag{2}$$

$$E_{yy} = \frac{\partial u}{\partial y} + \frac{1}{2}\left[\left(\frac{\partial u}{\partial y}\right)^2 + \left(\frac{\partial v}{\partial y}\right)^2 + \left(\frac{\partial w}{\partial y}\right)^2\right] \quad (3)$$

In these equations, *u, v, and w* are the displacements in the *x, y, and z* directions. *Exx* is the normal Lagrangian strain in the x direction while *Eyy* is the normal Lagrangian strain in the y direction.

Stiffness and elastic modulus were calculated as the maximum slope of the load-displacement curve and the stress-strain curve, respectively, for each of the two anatomic directions (Figures 12-13). 30% of the total data points were used as the starting and ending points for slope calculations, ex: total data points*0.3, designated *p*. 30% was chosen as the criterion on the basis of a previous study testing diseased PD tissue from this lab. Stiffness was calculated using equation 4, and the elastic modulus was calculated using equation 5 for all available data points between the boundaries of 15-85% of the collected data (initiation of test: 0%, final collected point: 100%) [26]. The largest slope calculated from the load-displacement curve and stress-strain curve was designated the stiffness and elastic modulus, respectively [Appendix A].

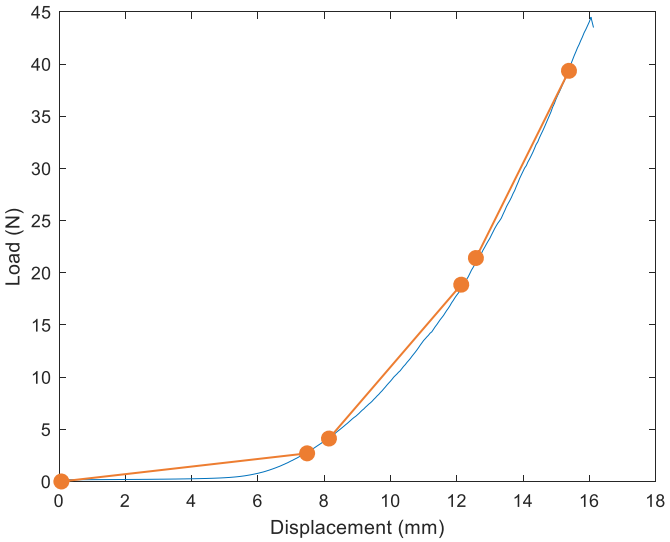

Figure 12: Load-displacement curve with three sample stiffness calculation ranges. Each range depicted consists of 30% of the total number of data points.

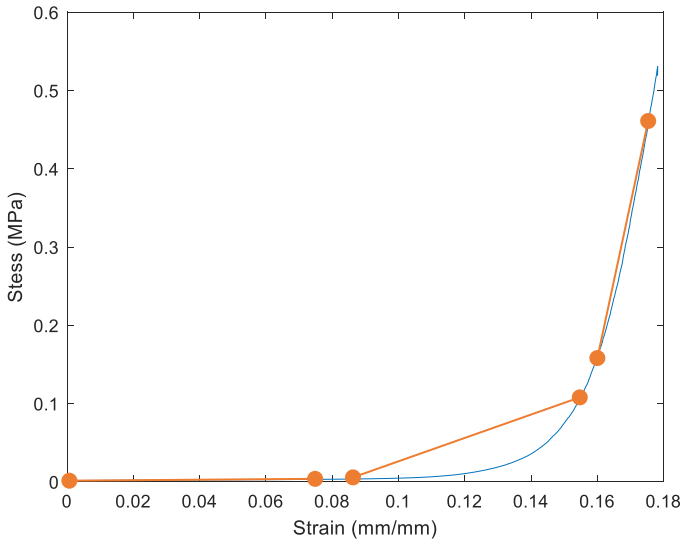

Figure 13: Stress-strain curve with three sample elastic modulus calculation ranges. Each range depicted consists of 30% of the total number of data points.

$$stiffness = \frac{load\ at\left(i+\frac{p}{2}\right) - load\ at\left(i-\frac{p}{2}\right)}{displacement\ at\left(i+\frac{p}{2}\right) - displacement\ at\left(i-\frac{p}{2}\right)} \tag{4}$$

$$elastic\ modulus = \frac{stress\ at\left(i+\frac{p}{2}\right) - stress\ at\left(i-\frac{p}{2}\right)}{strain\ at\left(i+\frac{p}{2}\right) - strain\ at\left(i-\frac{p}{2}\right)} \tag{5}$$

In order to objectively identify an inflection point between the toe region and the linear region of each stress-strain curve, each data point in the ramp, *i,* was fitted by assuming an exponential curve for the data before this point (Eq. 6) while the data after this point was modeled as a line [29] (Eq. 7).

$$\sigma = A\ (e^{B\,\varepsilon} - 1) \tag{6}$$

$$\sigma = m\,\varepsilon + q \tag{7}$$

In equation 6 and 7, σ is stress and ε is normal Lagrangian strain. *A, B, m*, and q are constants that were calculated with the code.

These equations are simply a means to describe the *shape of the curve*, and not to mathematically model the biaxial mechanical behavior. The data point that yielded the highest R squared value from *fittype* in Matlab for both equations (6) and (7) was

designated the inflection point. Normal Lagrangian strain at the inflection point was recorded for further analysis. Code used for the aforementioned calculations are provided in Appendix A.

Percent relaxation was also calculated. The biaxial tension test required that both directions reached the maximum load of 45 N; however, the first direction to reach the peak load would begin to relax while the second direction was still being loaded in tension. As seen in Figure 14, this created a secondary drop (as indicated by the arrow in the figure) in the first direction.

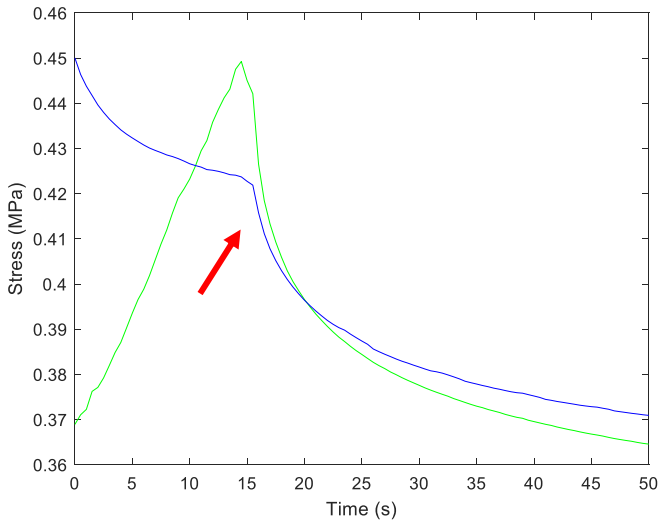

Figure 14: Example of the differing times at which peak load was attained for each axis as well as initial stress relaxation in a tissue sample. The arrow indicates the secondary drop in the direction which reaches the target 45N first. Green: longitudinal, blue: circumferential.

Although this issue was acknowledged and observed in every test, the "interrupted" relaxation was not considered in the calculations. The percent stress relaxation recorded was based on equation 8 where the peak stress was the stress measured upon attainment of 45 N and the equilibrium stress was that measured after 30 minutes from the peak, in each respective direction.

$$\%\ Relaxation\ = \frac{peak\ stress - equilibrium\ stress}{peak\ stress} * 100\% \tag{8}$$

Many factors led to variability in tissue, and in all tests, one direction would reach the maximum load before the other. If the tension test were to be stopped when the primary direction reached the maximum load, vital information could be overlooked or miscalculated in the secondary direction. Therefore, although the tissue was tested biaxially, the values calculated for analysis were considered independently, and material properties were calculated with the full 45N data inclusive in both directions.

2.4. Statistical Analysis

Data were statistically analyzed using JMP Pro 14 (SAS, Cary, NC). The independent variables were direction and ramp number while the dependent variables were stiffness, elastic modulus, strain at inflection point, and percent relaxation. A two-way ANOVA was performed on the averaged ranks of each variable to determine whether the dependent variables were dependent on directions and ramp number. Sample number was added as a random effect. Statistical significance was assumed for a p value less than 0.05.

3. Results

All graphs and data are represented in Figures 15-23.

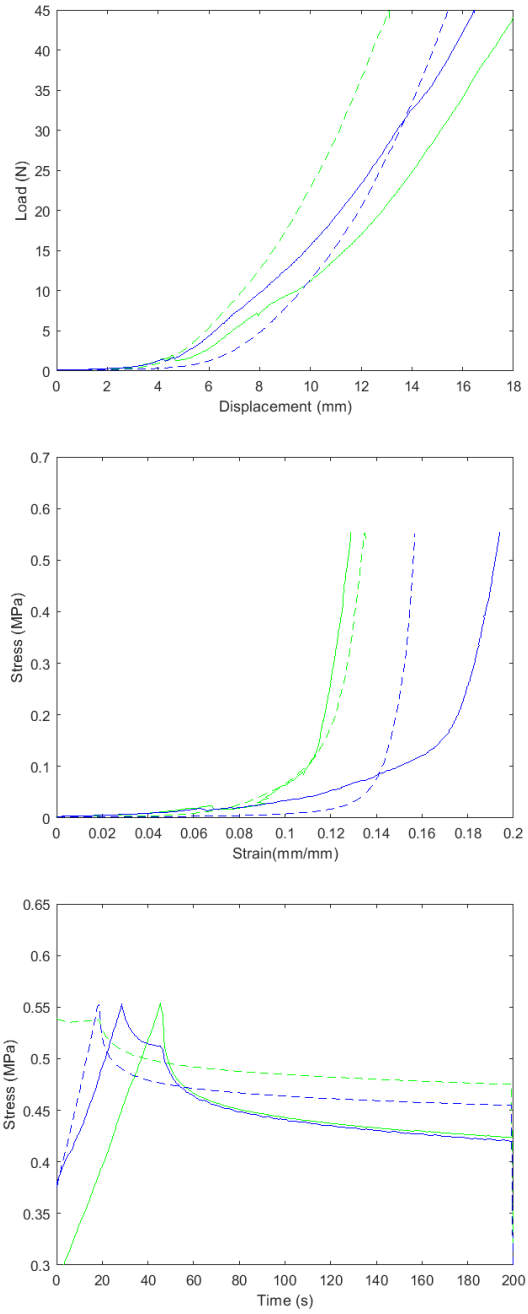

Figure 15: Top: load-displacement, middle: stress-strain, bottom: stress relaxation graphs for sample 101D.
Green: longitudinal, blue: circumferential.
Solid line: ramp 1, dotted line: ramp 2.

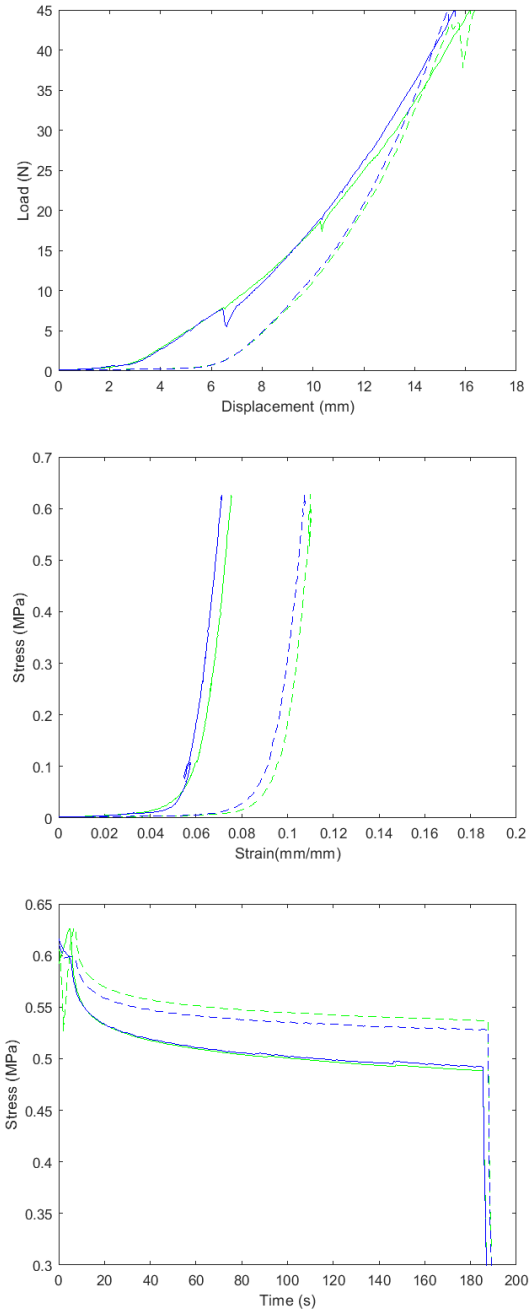

Figure 16: Top: load-displacement, middle: stress-strain, bottom: stress relaxation graphs for sample 684P**.**
Green: longitudinal, blue: circumferential.
Solid line: ramp 1, dotted line: ramp 2.

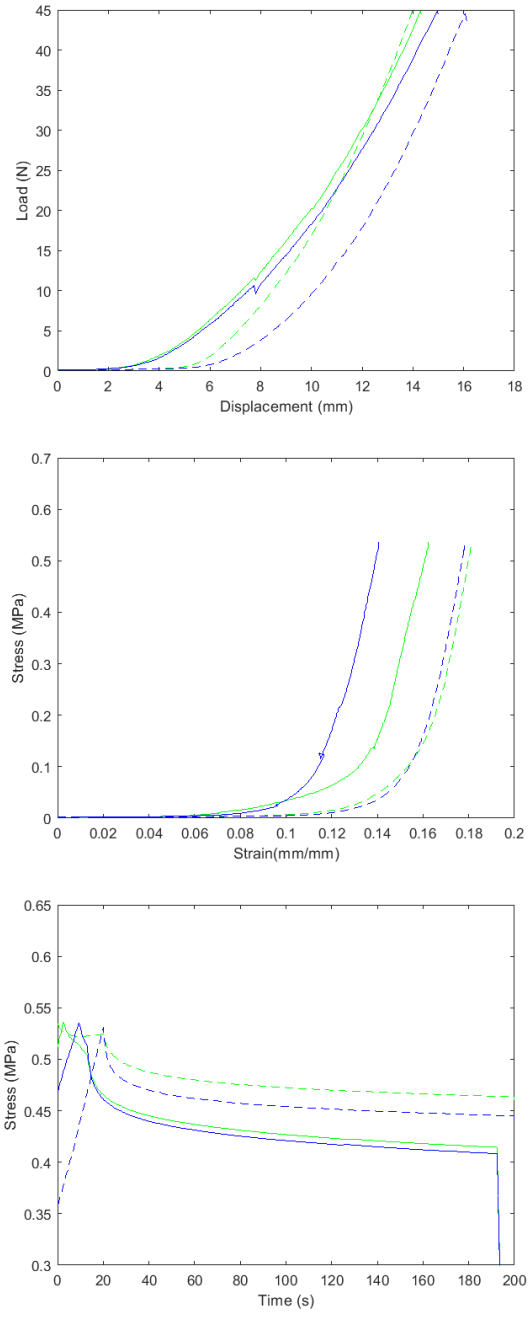

Figure 17: Top: load-displacement, middle: stress-strain, bottom: stress relaxation graphs for sample 774P
Green: longitudinal, blue: circumferential.
Solid line: ramp 1, dotted line: ramp 2.

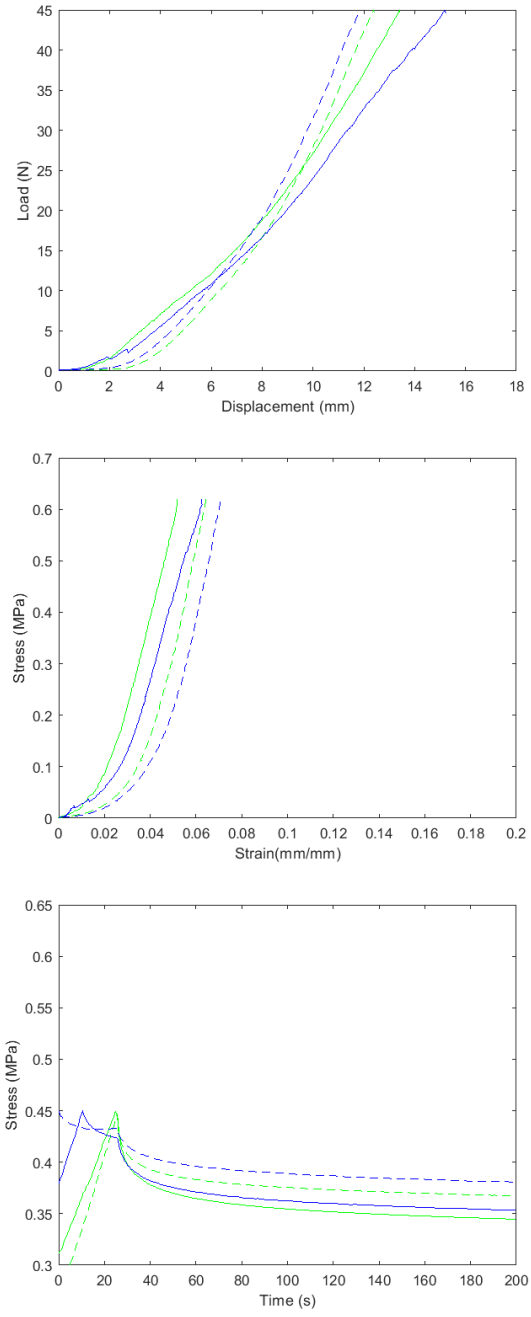

Figure 18: Top: load-displacement, middle: stress-strain, bottom: stress relaxation graphs for sample 895D
Green: longitudinal, blue: circumferential.
Solid line: ramp 1, dotted line: ramp 2.

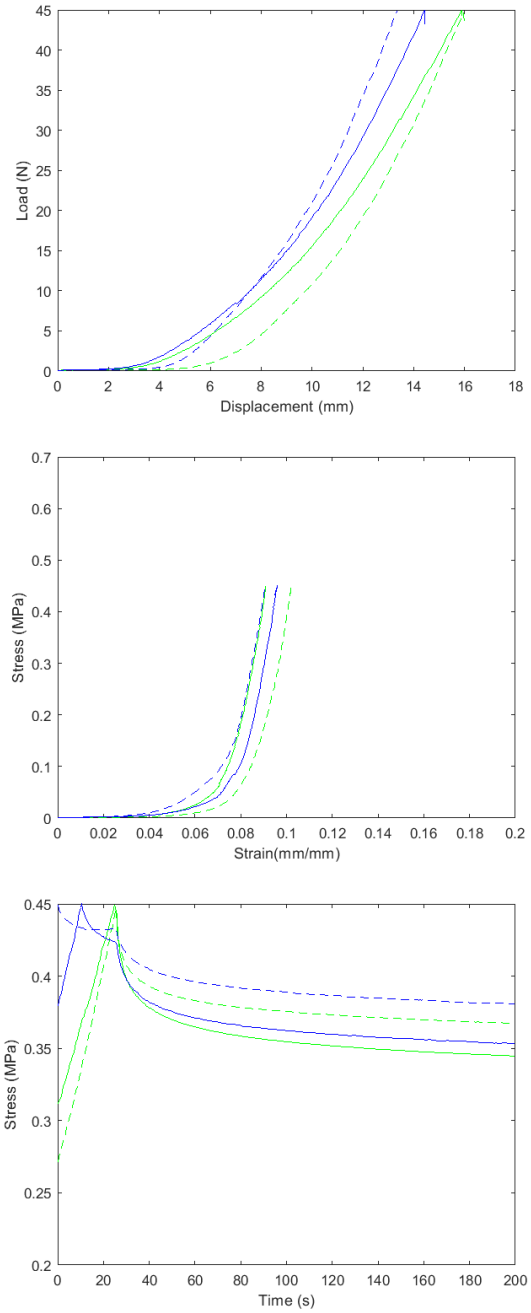

Figure 19: Top: load-displacement, middle: stress-strain, bottom: stress relaxation graphs for sample 895P
Green: longitudinal, blue: circumferential.
Solid line: ramp 1, dotted line: ramp 2.

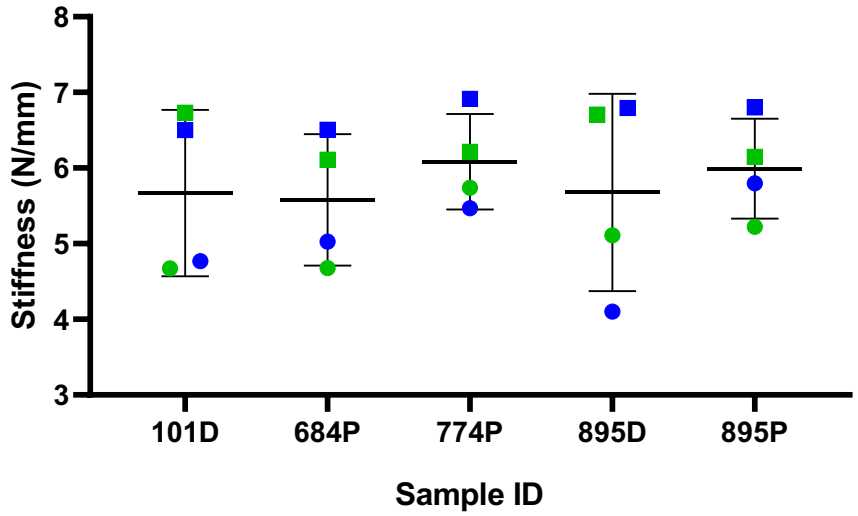

Figure 20: Scatter plot of stiffness (N/mm) data with mean and standard deviation bars. Circle: ramp 1, square: ramp 2, blue: longitudinal, green: circumferential.

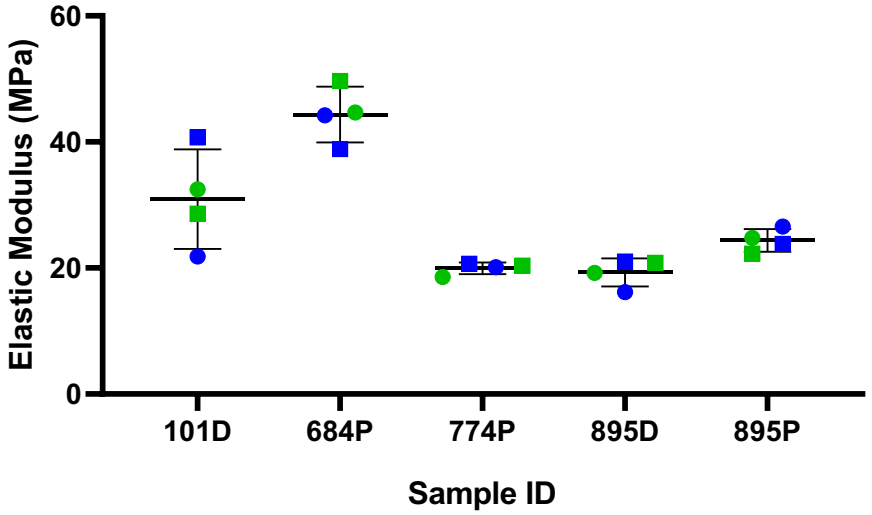

Figure 21: Scatter plot of elastic modulus (MPa) data with mean and standard deviation bars. Circle: ramp 1, square: ramp 2, blue: longitudinal, green: circumferential.

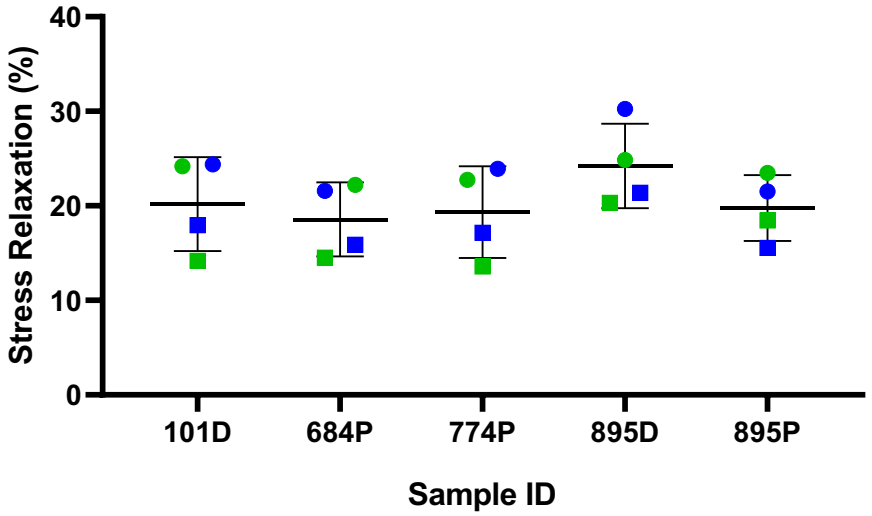

Figure 22: Scatter plot of stress relaxation (%) data with mean and standard deviation bars. Circle: ramp 1, square: ramp 2, blue: longitudinal, green: circumferential.

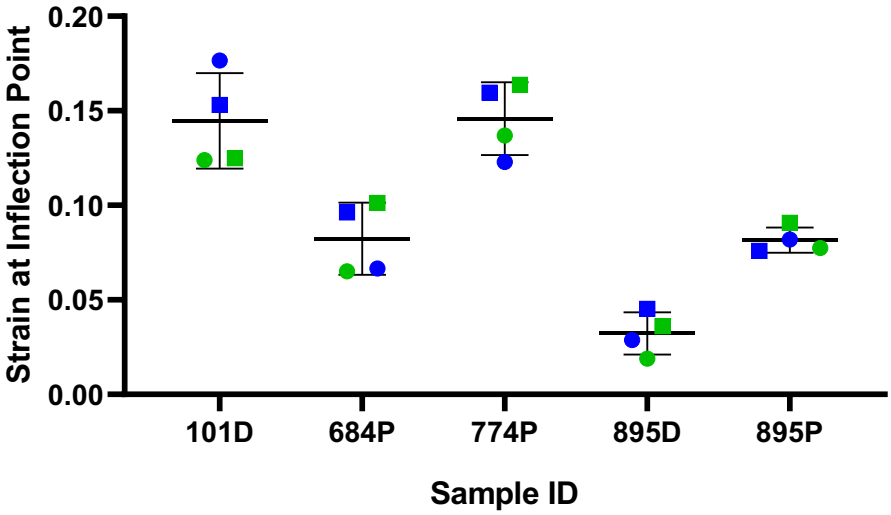

Figure 23: Scatter plot of strain at inflection point data with mean and standard deviation bars. Circle: ramp 1, square: ramp 2, blue: longitudinal, green: circumferential.

3.1. Linear Region Stiffness

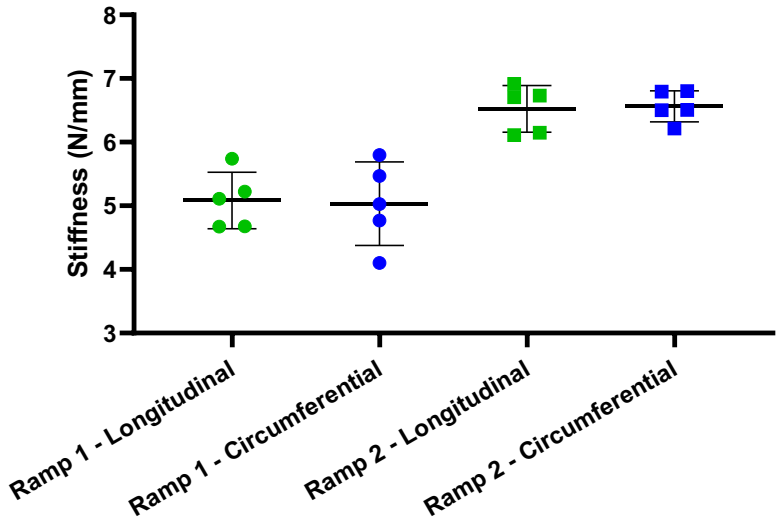

Figure 24: Scatterplot of stiffness (N/mm) data between ramp number and direction, with mean and standard deviation bars.

The data from Figure 24 showed that there was no statistically significant difference in the stiffness of the tissue between the longitudinal and circumferential direction ($p = 0.981$). However, between ramp 1 and ramp 2, there was a statistically significant increase in stiffness ($p < 0.0001$).

3.2. Elastic Modulus

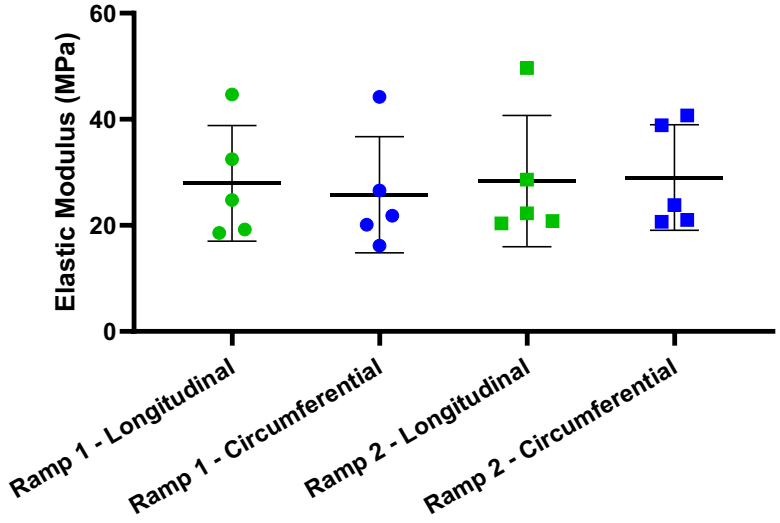

Figure 25: Scatterplot of elastic modulus (MPa) data between ramp direction and direction, with mean and standard deviation bars.

The modulus of elasticity data (Figure 25) showed no statistically significant difference between the longitudinal and circumferential direction ($p = 0.381$) or between ramp 1 and ramp 2 ($p = 0.719$).

3.3. Percent Stress Relaxation

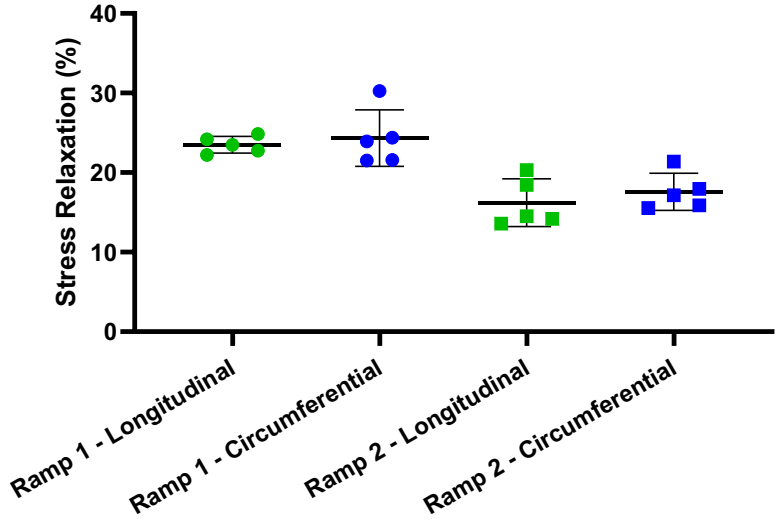

Figure 26: Scatterplot of percent stress relaxation data, presented by ramp number and direction, with mean and standard deviation bars.

Stress relaxation of the samples were measured after both directions reached the maximum load of 45N. The tissues were held at the displacement measured at the peak load, however the strains at which the stress relaxation was recorded were not consistent between samples. The strain at which the stress relaxation occurred was considered a covariant in the statistical calculations. The data from Figure 26 showed that there was no statistically significant difference in the percentage stress relaxation between the longitudinal and circumferential direction ($p = 0.461$). There was a statistically significant decrease in stress relaxation between ramp 1 and ramp 2 ($p < 0.0001$).

3.4. Strain at Inflection

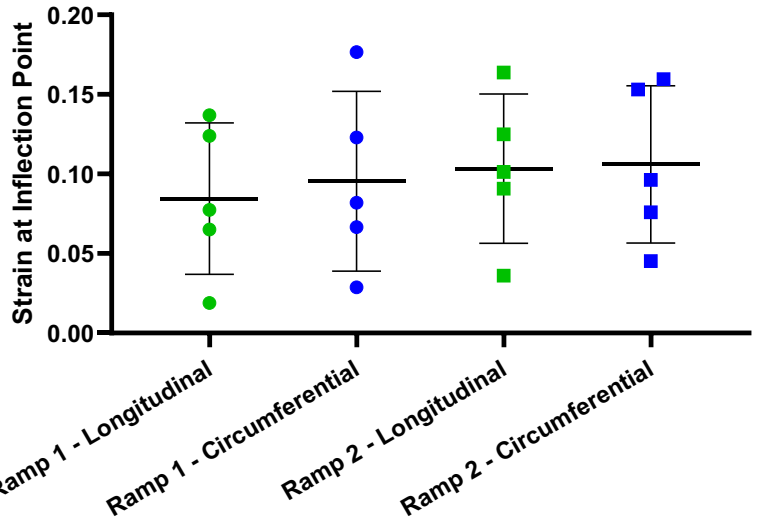

Figure 27: Scatterplot of the strain at inflection point, plotted by ramp number and direction, with mean and standard deviation bars.

The inflection points determined using the aforementioned approach (intersection of linear and exponential curves) corresponded to different loads/stresses, therefore, the load at the inflection point was considered as a covariant for a more objective comparison. At the inflection point the strain (Figure 27) showed a statistically significant increase between ramp 1 and ramp 2 ($p = 0.048$) but showed no statistically significant difference between the longitudinal and circumferential direction ($p = 0.551$).

The DIC strain maps were studied in order to examine potential differences in strain patterns. As noted, the stiffness of the TA tissue increases between the two ramps, so it is expected that for the second ramp, a larger load is required to reach the same strain from the first ramp. We examine the strain maps at the inflection point of each ramp as a comparison point. In these figures, the longitudinal direction is denoted by the green arrows while the circumferential direction is denoted by the blue arrows.

101 D			
Ramp 1 Inflection Point			
Longitudinal Strain		Circumferential Strain	
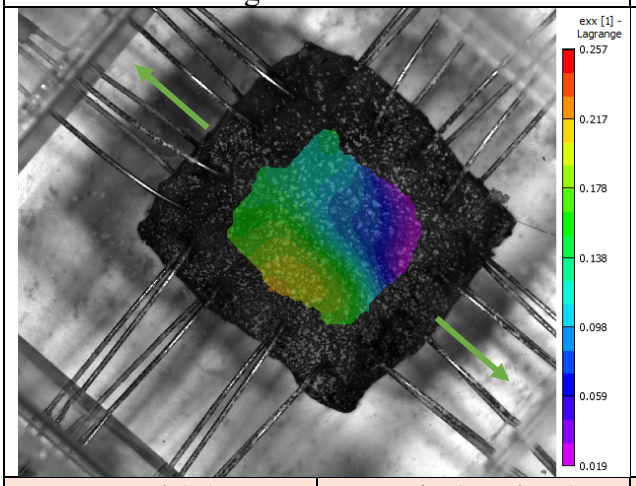		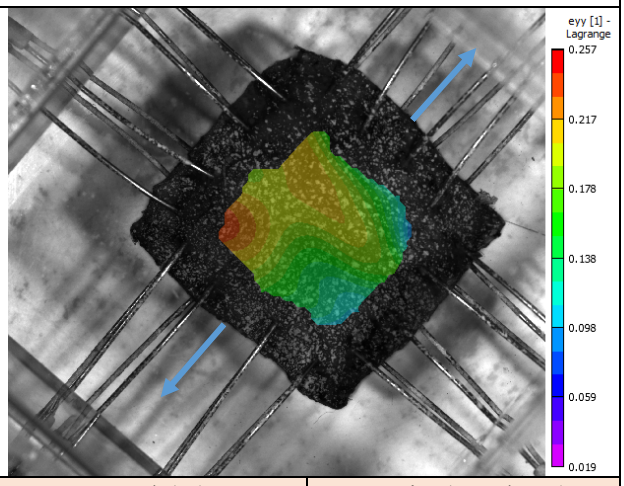	
Load (N)	Strain (mm/mm)	Load (N)	Strain (mm/mm)
30.272	0.124	17.025	0.177
Ramp 2 Inflection Point			
Longitudinal Strain		Circumferential Strain	
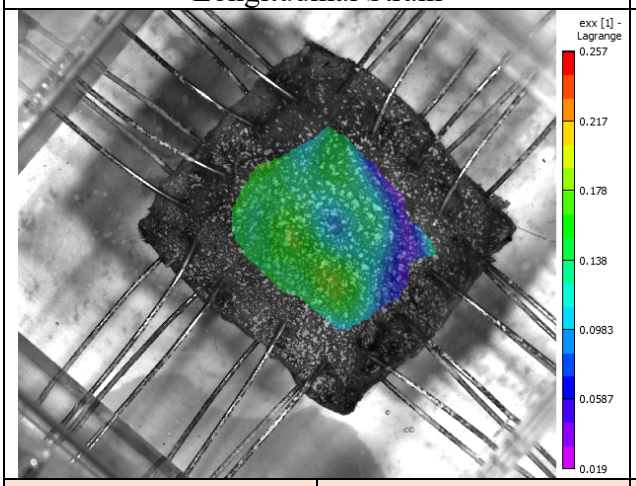		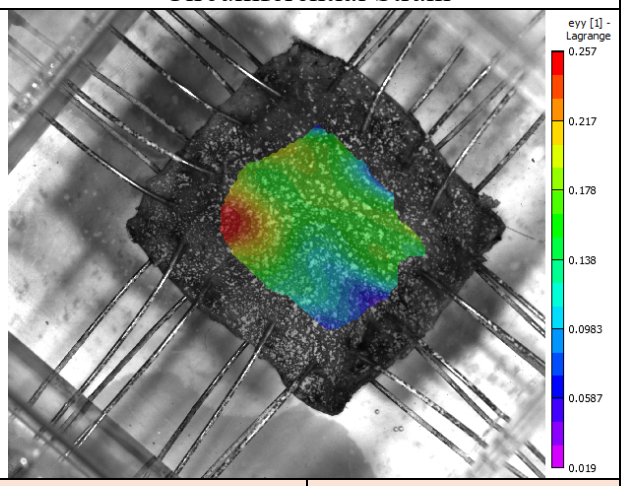	
Load (N)	Strain (mm/mm)	Load (N)	Strain (mm/mm)
20.245	0.125	26.585	0.153

Figure 28: DIC strain map at the inflection point in both directions for ramp 1 and ramp 2 for sample 101D, with corresponding load and strain values. In the first ramp, the circumferential direction reached maximum load of 45 N first, while in the second ramp, the longitudinal direction reached the maximum load of 45 N first.

In the longitudinal direction at the inflection point during ramp 2, a lower load is required to reach the same strain that was measured in the first ramp. However, in the circumferential direction, the opposite is true where in the second ramp a higher load is required to reach a lower strain compared to the first ramp (Figure 28)

684 P			
Ramp 1 Inflection Point			
Longitudinal Strain		Circumferential Strain	
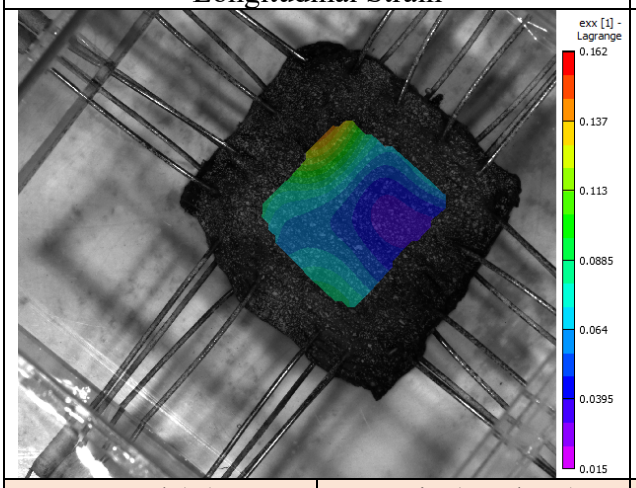		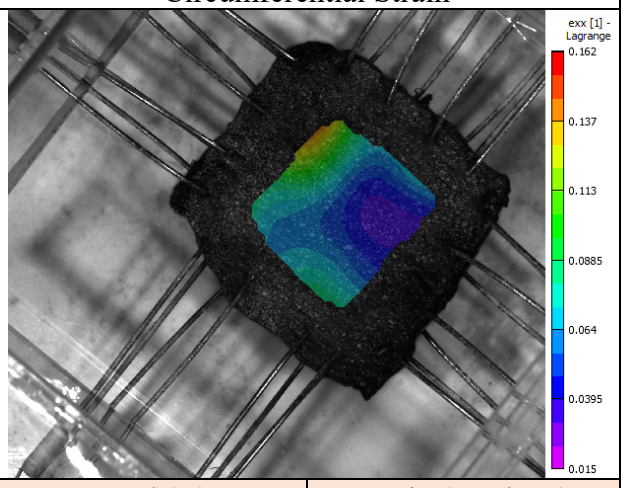	
Load (N)	Strain (mm/mm)	Load (N)	Strain (mm/mm)
15.476	0.0651	29.843	0.0667
Ramp 2 Inflection Point			
Longitudinal Strain		Circumferential Strain	
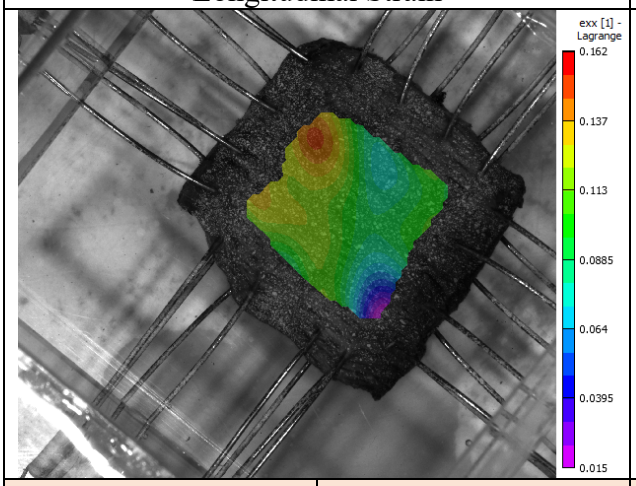		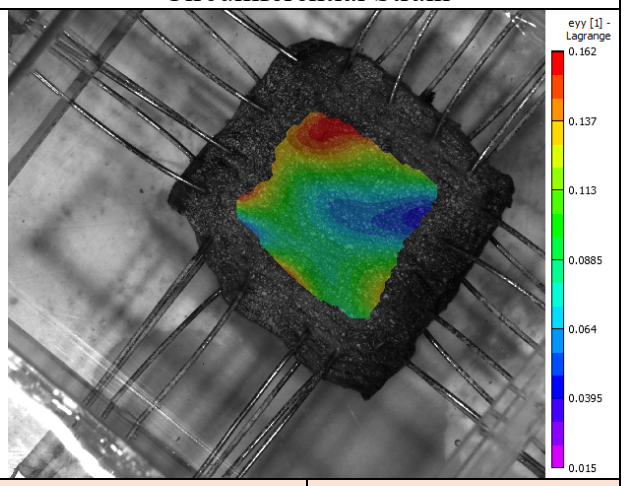	
Load (N)	Strain (mm/mm)	Load (N)	Strain (mm/mm)
15.357	0.101	13.979	0.0963

Figure 29: DIC strain map at the inflection point in both directions for ramp 1 and ramp 2 for sample 684P, with corresponding load and strain values. In the first ramp, the longitudinal direction reached maximum load of 45 N first, while in the second ramp, the circumferential direction reached the maximum load of 45 N first.

In sample 684P, the longitudinal direction did not show the stiffening that was expected, as the tissue reached a much higher strain in the second ramp compared to the first at a similar load. The same occurred in the circumferential direction between ramps where the sample required a lower load to reach a higher strain (Figure 29).

774 P			
Ramp 1 Inflection Point			
Longitudinal Strain		Circumferential Strain	
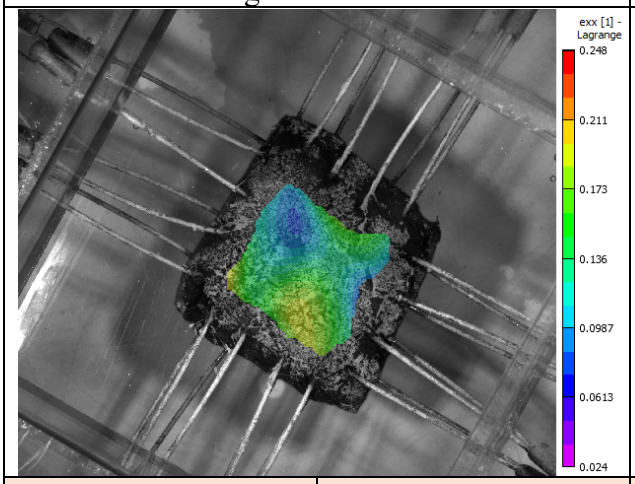		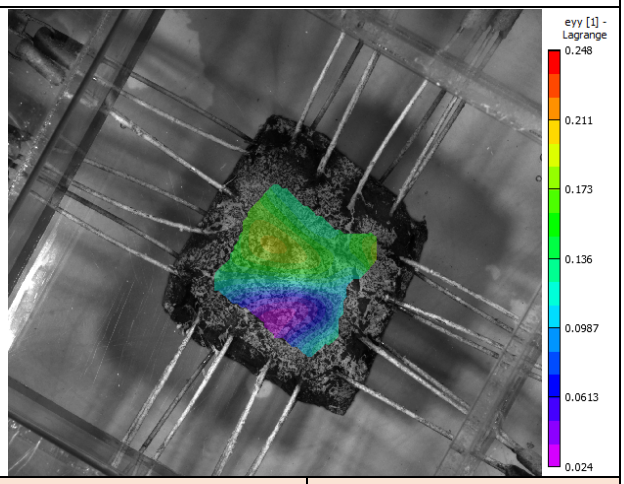	
Load (N)	Strain (mm/mm)	Load (N)	Strain (mm/mm)
11.146	0.137	17.713	0.123
Ramp 2 Inflection Point			
Longitudinal Strain		Circumferential Strain	
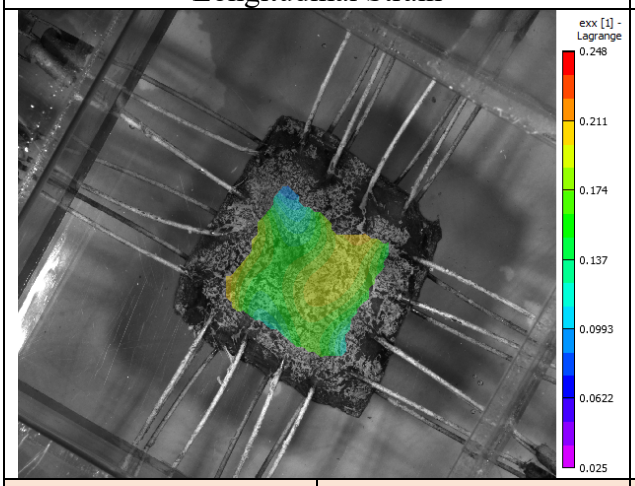		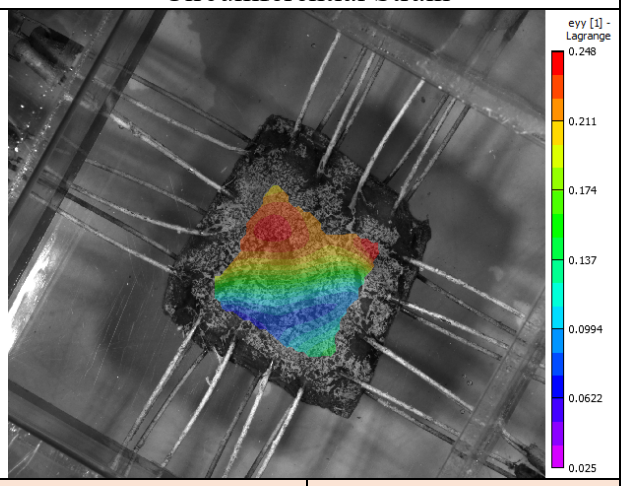	
Load (N)	Strain (mm/mm)	Load (N)	Strain (mm/mm)
15.105	0.164	13.054	0.160

Figure 30: DIC strain map at the inflection point in both directions for ramp 1 and ramp 2 for sample 774P, with corresponding load and strain values. In the first and second ramp, the longitudinal direction reached the maximum load of 45 N first.

In the longitudinal direction of sample 774P, a higher load is needed to reach the strain recorded at the inflection point of the first ramp. In the circumferential direction, the opposite can be observed, where a lower load in the second ramp is needed to measure a higher strain. (Figure 30).

895 D			
Ramp 1 Inflection Point			
Longitudinal Strain		Circumferential Strain	
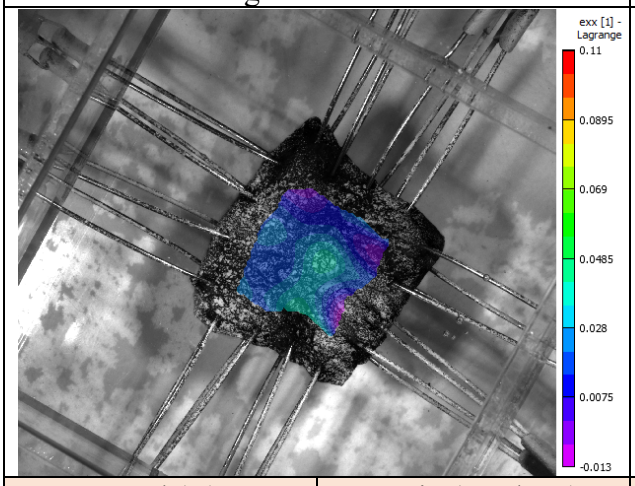		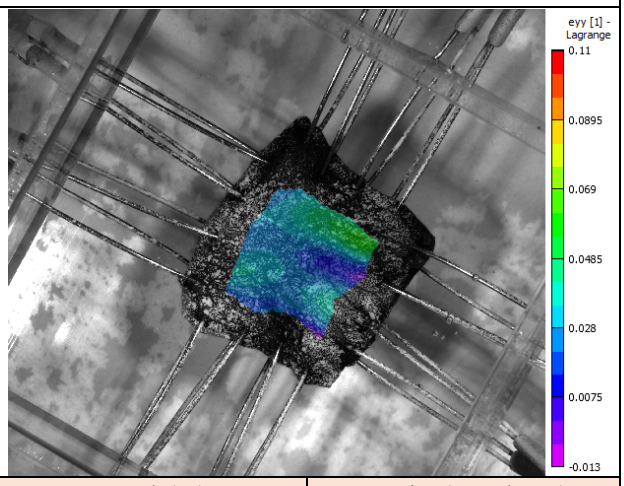	
Load (N)	Strain (mm/mm)	Load (N)	Strain (mm/mm)
5.741	0.0189	8.563	0.0288
Ramp 2 Inflection Point			
Longitudinal Strain		Circumferential Strain	
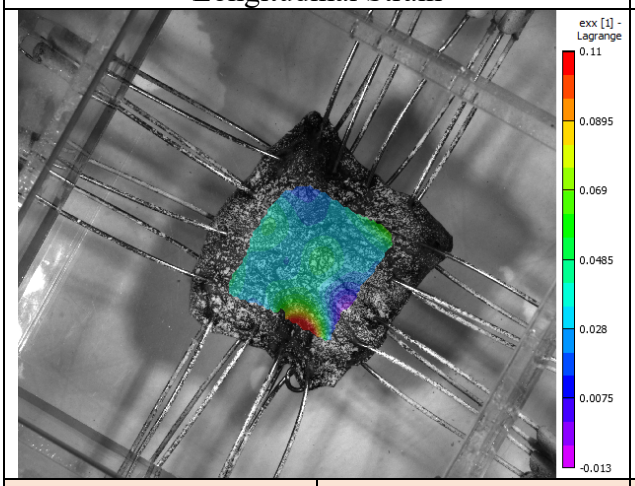		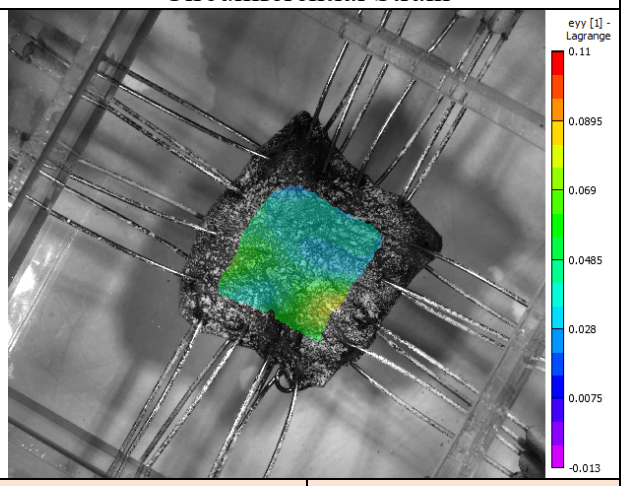	
Load (N)	Strain (mm/mm)	Load (N)	Strain (mm/mm)
8.331	0.0361	11.142	0.0453

Figure 31: DIC strain map at the inflection point in both directions for ramp 1 and ramp 2 for sample 895D, with corresponding load and strain values. In the first and second ramp, the longitudinal direction reached the maximum load of 45 N first.

In both the longitudinal and circumferential directions of sample 895D, a lower load in the second ramp is required to attain a similar strain from the first ramp. (Figure 31).

895 P			
Ramp 1 Inflection Point			
Longitudinal Strain		Circumferential Strain	
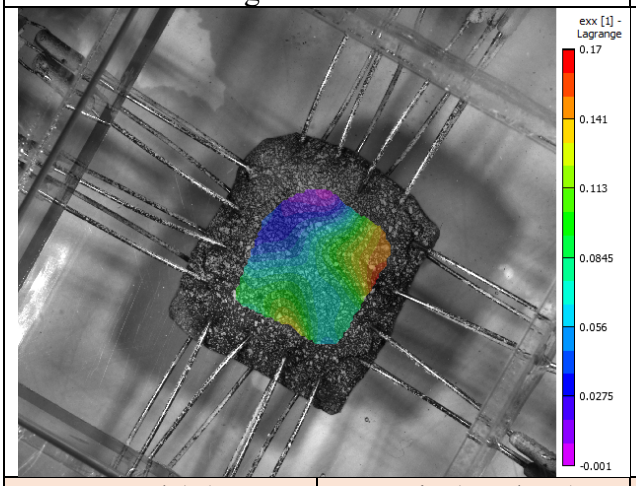		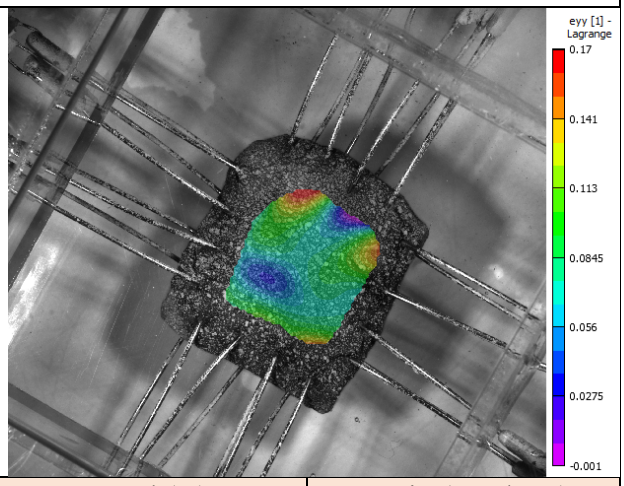	
Load (N)	Strain (mm/mm)	Load (N)	Strain (mm/mm)
14.040	0.0774	12.923	0.0820
Ramp 2 Inflection Point			
Longitudinal Strain		Circumferential Strain	
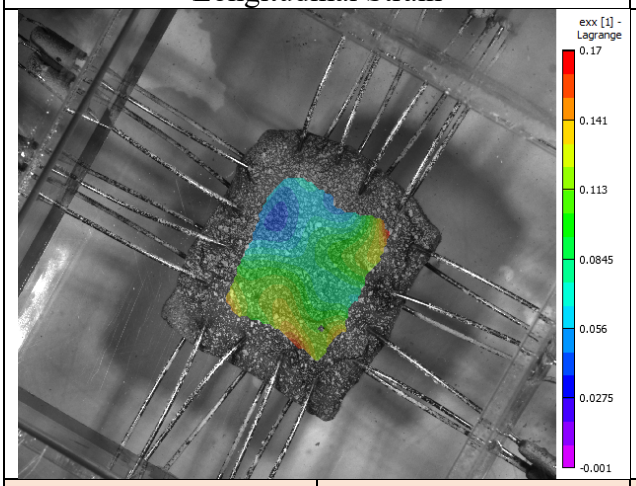		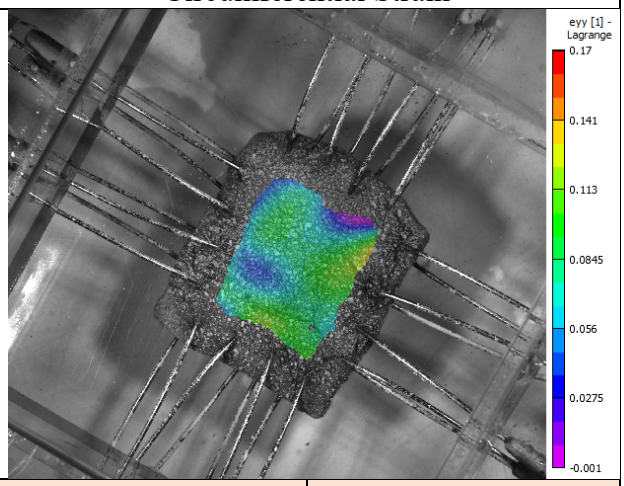	
Load (N)	Strain (mm/mm)	Load (N)	Strain (mm/mm)
18.459	0.0907	13.495	0.0759

Figure 32: DIC strain mapping at the inflection point in both directions for ramp 1 and ramp 2 for sample 895P, with corresponding load and strain values. In the first and second ramp, the circumferential direction reached the maximum load of 45 N first.

In the last sample, 895P, in both the longitudinal and circumferential directions, a higher load is needed in the second ramp in order to acquire a comparable strain to the first ramp (Figure 32).

Based on the 5 tissue samples, comparisons between ramp 1 and ramp 2 revealed that the TA was neither stiffer (higher load for similar strain) nor less stiff (lower load for similar strain). Since the stiffness of the tissue increases between ramps and this is not shown at the inflection point which is normally at lower loads relative to the peak load of 45N, it can be deduced that the larger changes in tissue mechanics would occur at higher loads where the linear region exists. This is consistent with observations from previous studies which found that stiffening of soft connective tissues with acellular collagen constructs occurs in the linear region relative to the toe region [30].

4. Discussion

The objectives of this study were to quantify the elastic and viscoelastic properties of the non-diseased human TA. TA tissue was dissected from human donors and prepared as 3 cm by 3 cm samples for biaxial biomechanical characterization. The tissue samples were loaded in tension simultaneously in two anatomic directions up to a prescribed load of 45N, allowed to stress relax in both directions, and following a recovery period, received the same loading protocol.

Overall, the results from this study indicate that the non-diseased TA tissue exhibits no statistically significant differences by anatomical directions (longitudinal and circumferential) with regard to stiffness, elastic modulus, normal strain at the inflection point, and percent stress relaxation. Hence, under the prescribed biaxial loading conditions, TA tissue exhibits mechanical isotropy, though the additional of more samples to the analysis would be help to confirm these observations. Additionally, there was no statistically significant difference in elastic modulus between the two ramps.

Statistically significant differences between ramp 1 and ramp 2 were observed for linear stiffness, percent stress relaxation, and strain at the inflection point. The stiffness of the non-diseased tissue increases while the percent stress relaxation decrease, as detailed in Table 3.

		Longitudinal	Circumferential
Stiffness	Ramp 1	5.08 ± 0.44	5.03 ± 0.65
	Ramp 2	6.52 ± 0.37	6.56± 0.24
Percent Stress Relaxation	Ramp 1	22.0 ± 2.6	22.5 ± 75.3
	Ramp 2	17.7 ± 5.0	19.4 ± 3.5

Table 3: Mean values with standard deviation for stiffness, strain at inflection, and percent stress relaxation for the longitudinal and circumferential direction in both ramps.

A comparison can be made between the biaxial material properties of non-diseased TA tissue and previous data (generated by our research group) for biopsied PD plaques as well as pericardium graft [26], which is often used for PD surgical reconstruction. The previous study used the same protocol to prepare the samples as well as preconditioning, however, the testing protocol involved loading the sample 3 times sequentially, without the stress relaxation, but allowing 15 minutes for recovery between ramps. Hence, data from only the first ramp were compared between the non-diseased (current study) and PD tissue [26]. A two-way ANOVA was performed on the averaged ranks of for both stiffness and modulus to compare the non-diseased TA to the diseased PD plaques as well as the non-diseased TA to the pericardium graft (Figures 33 and 34).

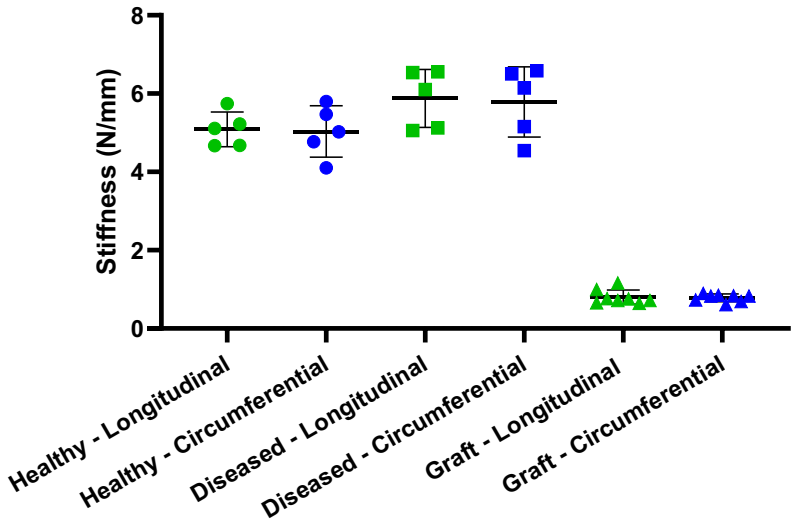

Figure 33: Stiffness (N/mm) of healthy vs diseased (PD) TA tissue vs pericardium graft material, with mean and standard deviation bars.

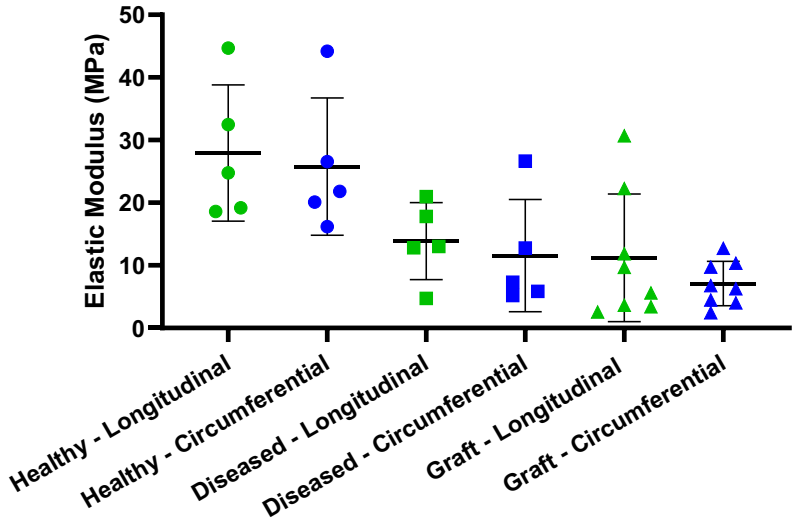

Figure 34: Elastic modulus (MPa) of healthy vs diseased (PD) TA tissue vs pericardium graft material, with mean and standard deviation bars.

The non-diseased TA tissue exhibited a lower stiffness in comparison to the PD plaques ($p = 0.0409$), but a higher stiffness than the pericardium graft tissue ($p < 0.0001$). The healthy tissue also differs from the diseased PD plaques and graft tissue when comparing the elastic modulus ($p = 0.0028$, $p < 0.0001$, respectively) [23]. The TA tends to ossify during the onset of PD, so the result from the stiffness comparison is congruent with this assumption. However, further research needs to be done in regards to the results from the elastic modulus comparison, in particular, taking into account the varying thickness of the tissue with more precise dissection. The graft tissue has a vastly different stiffness compared to the healthy TA tissue, further confirming the necessity to create a graft that can better approximate the properties of the healthy TA.

The results from this study can also be compared to the previous studies done on the material properties of the human TA. The elastic modulus of the healthy TA when loaded uniaxially to rupture resulted in values around 100 MPa, considerably higher than the average elastic modulus found in the current study (32.92 ± 16.74 MPa) [15]. As seen from the elastic modulus data from this study, the values have a wide range and the number of samples are low, both of which can be the reason for the discrepancy between studies. The previous uniaxial rupture study tested tissues from donors within 12-24 hours from death [15], whereas the current study tested tissues which had gone through multiple freeze-thaw cycles. The introduction of multiple freeze-thaw cycles can lower the elastic modulus of the biological material [31].

Based on the outcome of this study, it can be concluded that the TA tissue becomes stiffer and relaxes less after being pulled in tension up to 45 N. Previous work has reported that an increased number of cycles in fatigue loading of tendons also resulted in higher stiffness [32]. The stiffness increase is found on the observation that mechanical cyclic tensile loading increases the strength of the collagen crosslink thereby increasing the effective stiffness of the fibrils [30].

This study provides a benchmark for testing non-diseased TA tissue as well as a preliminary understanding of the material properties of the tissue. Still, there were several study limitations. The donor organs from UTN arrived in insulated packaging with dry ice, were immediately place in the freezer in lab, but will still undergo freeze thaw cycles which can affect the material properties of the tissue [31]. Another limitation is that the tissue is tested ex vivo rather than in vivo. In vivo, tissues that experience loading can induce cellular signaling events that affect collagen structure, but this would not occur when testing tissues ex vivo [30]. The non-diseased TA tissue was also tested only to 45 N because of the limitations of the equipment. Equipment that would allow further tension possibly to rupture could provide more information on the behavior of the tissue. Creep testing can also be done on the non-diseased TA to provide more information on the viscoelasticity of the tissue.

Though the sample size for this study is low, future work can expand upon this work with additional samples. Results from this study can be used to identify suitable grafts which more closely match TA properties, since it can be seen from this study that the material properties of non-diseased TA tissue are different from the current graft standard. This can, in turn, aid in better recovery and patient satisfaction which currently is only at 72.4 % [11]. The stiffening of the tissue after a succeeding ramp can be an important factor with PTT surgery, as the penis will have to go through multiple treatments of loading. Stress relaxation properties of the TA can also be beneficial for designing the treatment protocols of PTT, as the practice involves not only the number of treatments, but the duration of treatments.

References

[1] G. Brock, G. L. Hsu, L. Nunes, B. V. Heyden, T. F. Lue, "The anatomy of the tunica albuginea in the normal penis and peyronie's disease," *The Journal of Urology.,* vol. 157, pp. 276-281, 1997.

[2] A. Gefen, D. Elad, and J. Chen, "Biomechanical aspects of Peyronie's disease in development and following reconstructive surgeries," *International Journal of Impotence Research.*, vol. 14, pp. 389-396, 2014.

[3] L. A. Levine, "The Clinical and Psychosocial Impact of Peyronie's Diease," *Am J Manag Care*., vol. 19, pp 55-61, 2013.

[4] B. A. Sherer, K. F. Godlewski, and L. A. Levine, "Pharmacologic therapy for Peyronie's disease: what should we prescribe?," *Expert Opin. Pharmacother.,* vol. 15, no. 9, pp. 1299-1311, 2015.

[5] T. C. Peak, G. C. Mitchell, F. A. Yafi, and W. J. Hellstrom, "Role of collagenase clostridium histolyticum in Peyronie's disease," *Biol. Targets Ther.*, vol. 9, pp. 107–116, 2015.

[6] A. Gefen, J. Chen, D. Elad, "Structural Analysis of the Human Penis during Erection,".

[7] D. B. Dibenedetti, D. Nguyen, L. Zografos, R. Ziemiecki, and X. Zhou, "A population-based study of peyronie's disease: Prevalence and treatment patterns in the United States," *Adv. Urol.*, vol. 2011, pp. 10–13, 2011.

[8] F. Sommer, U. Schwarzer, G. Wassmer, W. Bloch, M. Braun, T. Klotz, U. Engelmann, "Epidemiology of Peyronie's disease," *International Journal of Impotence Research*., vol. 14, pp. 379-383, 2002.

[9] G. Cavallini, and G. Paulis, "Peyronie's Disease, A Comprehensive Guide," 2015.

[10] A. A. Hussein, A. Alwaal, and T. F. Lue, "All about Peyronie's disease," *Asian J. Urol.*, vol. 2, no. 2, pp. 70–78, 2015.

[11] D. Papagiannopoulos, E. Yura, and L. Levine, "Examining Postoperative Outcomes after Employing a Surgical Algorithm for Management of Peyronie's Disease: A Single-Institution Retrospective Review," *International Society for Sexual Medicine*., vol. 12, pp. 1474-1480, 2015.

[12] G. Hatzichristodoulou, "Grafting techniques for Peyronie's disease," *Transl. Androl. Urol.*, vol. 5, no. 3, pp. 334–341, 2016.

[13] L. A. Levine, M. Newell, F. L. Taylor, "Penile traction therapy for treatment of Peyronie's disease: a single-center pilot study," *J Sex Med*., vol. 5, no. 6, pp 1468-1473, 2008.

[14] M. F. Usta and T. Ipekci, "Penile traction therapy for Peyronie's disease—what's the evidence?," *Transl. Androl. Urol.*, vol. 5, no. 3, pp. 303–309, 2016.

[15] M. Bitsch, B. Kromann-Andersen, J. Schou, E. Sjøntoft, "The elasticity and the tensile strength of tunica albuginea of the corpora cavernosa," *The Journal of Urology.,* vol. 143, pp. 642-645, 1990.

[16] G. L. Hsu, G. Brock, L. Martínez-Piñeiro, B. von Heyden, T. F. Lue, E. A. Tanagho, "Anatomy and strength of the tunica albuginea: its relevance to penile prosthesis extrusion," *The Journal of Urology.,* vol. 151, pp. 1205-1208, 1994.

[17] E, Akkus, S. Carrier, K. Baba, G. L. Hsu, H. Padma-Nathan, L. Nunes, T. F. Lue, "Structural alterations in the tunica albuginea of the penis: impact of Peyronie's disease, ageing and impotence," *British Journal of Urology*., vol. 79, pp. 47-53, 1997.

[18] M. S. Sacks, "Biaxial Mechanical Evaluation of Planar Biological Materials," *Journal of Elasticity*., vol. 61, pp. 199-246, 2000.

[19] K. Robi, N. Jakob, K. Matevz and V. Matjaz, "The Physiology of Sports Injuries and Repair Processes," *Current Issues in Sports and Exercise Medicine.*, 2013.

[20] N. McCormick and J. Lord, "Digital image correlation," *Mater. Today.*, vol. 13, no. 12, pp. 52–54, 2010.

[21] A. Baah-Dwomoh, M. Alperin, M. Cook, R. De Vita, "Mechanical Analysis of the Uterosacaral Ligament: Swine versus Human," *Annals of Biomedical Engineering.,* vol. 46, pp. 2036-2047, 2018.

[22] J. A. McGuire, C. L. Crandall, S. Abramowitch, R. De Vita, "Inflation and Rupture of Vaginal Tissue," *Interface Focus*., vol. 9, 20190029, 2019.

[23] J. A. McGuire, S. Abramowitch, S. Maiti, R. De Vita, "Swine Vagina Under Biaxial Loading: An Investigation of Large Deformations and Tears," *Journal of Biomechanical Engineering,* vol. 141, 041003, 2019.

[24] M. Palanca, G. Tozzi, and L. Cristofolini, "The use of digital image correlation in the biomechanical area: A review," *Int. Biomech.*, vol. 3, no. 1, pp. 1–21, 2016.

[25] A. L. Mescher, *Junqueira's Basic Histology*, 12th ed. McGraw-Hill Medical, 2009.

[26] D. Surinach, R. De Vita, L. Levine, V. M. Wang, "Biaxial Mechanical Properties of Tutoplast Processed Pericardial Grafts: Comparison to Human Tunica Albuginea Properties", Poster presentation, Biomedical Engineering Society (BMES), Phoenix, AZ, 2017.

[27] "digitalimagecorrelation.org," *digitalimagecorrelation.org*. [Online]. Available: https://digitalimagecorrelation.org/.

[28] Y. C. Fung, P. Tong, and X. H. Chen, *Classical and computational solid mechanics*. New Jersey: World Scientific, 2017.

[29] M. L. Tanaka, C. A. Weisenbach, M. C. Miller, L. Kuxhaus, "A Continuous Method to Compute Model Parameters for Soft Biological Materials," *Journal of Biomechanical Engineering.,* vol. 133, no. 7, 2011.

[30] M. L. Chen, J. W. Ruberti, T. D. Nguyen, "Increased stiffness of collagen fibrils following cyclic tensile loading", *Journal of the Mechanical Behavior of Biomedical Materials.,* vol. 82, pp. 345-354, 2018.

[31] H. Huang, J. Zhang, K. Sun, X. Zhang, S. Tian, "Effects of repetitive multiple freeze-thaw cycles on the biomechanical properties of human flexor digitorum superficialis and flexor pollicis longus tendons," *Clinical Biomechanics.,* vol. 26, no. 4, pp. 419-423, 2011.

[32] B. R. Freedman, A. Zuskov, J. J. Sarver, M. R. Buckley, L. J. Soslowsky, “Evaulating Changes in Tendon Crimp With Fatigue Loding as an Ex Vivo Structural Assessment of Tendon Damage,” *Orthopaedic Research Society.,* 2015

Appendix A: Matlab code used to calculate material properties

```
close all; clc;clear;

warning off;

p = 0.3; %percentage of data used

%% Read in and define relevent data

source_dir= 'source_directory';
%determine path to the folder that contains data

source_files = dir(fullfile(source_dir, '*filename_Data_PD.csv'));

data=xlsread(source_files.name); %read data file

%% LONGITUDINAL
    %% Load(Y) against Displacement (X)

    [s1, s2] = size(data);
    disp=data(2:s1,16);
    load=data(2:s1,9);
    strain=data(2:s1,2);
    stress=data(2:s1,13);

    [s3, s4]=max(disp); % max load ~ point of failure s3=max s4=position;
    disp_cut=disp(1:s4);
    load_cut=load(1:s4);
    strain_cut=strain(1:s4);
    stress_cut=stress(1:s4);

    [len]=length(disp_cut);

    index=transpose(1:1:len);

    w=round(p*len);
    h=round(w/2);

    %% Calculate max slope for stiffness and modulus

    guess_stiff=zeros(1,1-w-1);
    guess_mod=zeros(1,1-w-1);
    for j=h+1:(len-h-1)
        guess_stiff(j)=((load_cut(j+h)-load_cut(j-h))/(disp_cut(j+h)-disp_cut(j-h)));
        guess_mod(j)=((stress_cut(j+h)-stress_cut(j-h))/(strain_cut(j+h)-strain_cut(j-h)));

        j=j+1;
    end
    [max_stiff, loc_stiff]=max(guess_stiff);
    [max_mod, loc_mod]=max(guess_mod);

    load_stiff=load_cut(loc_stiff);
    load_mod=load_cut(loc_mod);
```

```
53
54      %% Piecewise curve fit for inflection point
55
56      rsq_exp=zeros(1,len-2);
57      rsq_lin=zeros(1,len-2);
58
59      ft_exp = fittype('a*(exp(b*x)-1)');
60      ft_lin = fittype('m*x+b');
61      for i=2:len-1
62
63          [f_exp,g_exp]= fit(strain_cut(1:i), stress_cut(1:i), ft_exp);
64          [f_lin,g_lin]= fit(strain_cut(i:len), stress_cut(i:len),ft_lin);
65
66          rsq_exp(i-1)=getfield(g_exp,'rsquare');
67          rsq_lin(i-1)=getfield(g_lin,'rsquare');
68      end
69
70      rsq_diff=2-rsq_exp-rsq_lin;
71
72      locations = find(rsq_diff < 0.01);
73
74      if length(locations)==0
75          locations(1) = find(rsq_diff == min(rsq_diff));
76      end
77
78     loc_inf = locations(1);
79
80     inflectionstrainL= strain_cut(loc_inf);
81
82     %% Display
83
84      display('Longitudinal Values')
85      display(['Stiffness is ' num2str(max_stiff) ' N/m'])
86      display(['Modulus is ' num2str(max_mod) ' MPa'])
87      display(['Strain at inflection point is ' num2str(inflectionstrainL)])
88      display([' '])
89
90  %% CIRCUMCERENTIAL
91      %% Load(Y) against Displacement (X)
92
93      [s1, s2] = size(data);
94      disp=data(2:s1,17);
95      load=data(2:s1,11);
96      strain=data(2:s1,3);
97      stress=data(2:s1,15);
98
99      [s3, s4]=max(disp); % max load ~ point of failure s3=max s4=position
100     disp_cut=disp(1:s4);
101     load_cut=load(1:s4);
102     strain_cut=strain(1:s4);
103     stress_cut=stress(1:s4);
104
105     [len]=length(disp_cut);
106
```

```
53
54      %% Piecewise curve fit for inflection point
55
56      rsq_exp=zeros(1,len-2);
57      rsq_lin=zeros(1,len-2);
58
59      ft_exp = fittype('a*(exp(b*x)-1)');
60      ft_lin = fittype('m*x+b');
61      for i=2:len-1
62
63          [f_exp,g_exp]= fit(strain_cut(1:i), stress_cut(1:i), ft_exp);
64          [f_lin,g_lin]= fit(strain_cut(i:len), stress_cut(i:len),ft_lin);
65
66          rsq_exp(i-1)=getfield(g_exp,'rsquare');
67          rsq_lin(i-1)=getfield(g_lin,'rsquare');
68      end
69
70      rsq_diff=2-rsq_exp-rsq_lin;
71
72      locations = find(rsq_diff < 0.01);
73
74      if length(locations)==0
75          locations(1) = find(rsq_diff == min(rsq_diff));
76      end
77
78     loc_inf = locations(1);
79
80     inflectionstrainL= strain_cut(loc_inf);
81
82     %% Display
83
84      display('Longitudinal Values')
85      display(['Stiffness is ' num2str(max_stiff) ' N/m'])
86      display(['Modulus is ' num2str(max_mod) ' MPa'])
87      display(['Strain at inflection point is ' num2str(inflectionstrainL)])
88      display([' '])
89
90  %% CIRCUMCERENTIAL
91      %% Load(Y) against Displacement (X)
92
93      [s1, s2] = size(data);
94      disp=data(2:s1,17);
95      load=data(2:s1,11);
96      strain=data(2:s1,3);
97      stress=data(2:s1,15);
98
99      [s3, s4]=max(disp); % max load ~ point of failure s3=max s4=position
100     disp_cut=disp(1:s4);
101     load_cut=load(1:s4);
102     strain_cut=strain(1:s4);
103     stress_cut=stress(1:s4);
104
105     [len]=length(disp_cut);
106
```

```
159     display('Circumferential Values')
160     display(['Stiffness is ' num2str(max_stiff) ' N/m'])
161     display(['Modulus is ' num2str(max_mod) ' MPa'])
162     display(['Strain at inflection point is ' num2str(inflectionstrainC)])
163     display([' '])
164
```

Appendix B: Standard Operating Protocol

Dissection

1) Organs are stored in the freezer until 48 hours prior to testing where they are removed and placed in the fridge to thaw.
2) 24 hours prior to testing, run the organ in a water bath to finish thawing while prepping the dissection tools and space.
    a) Tourniquet band
    b) Tweezers
    c) L shaped dissecting scissors
    d) Curved Kelly clamp
    e) Small dissection scissors
    f) Skin marking pen and ruler
    g) Size 10 scalpel
    h) Saline
    i) Thin tube ex. coffee straw
    j) Cutting board
    k) Large lab zip lock bag
    l) Small lab zip lock bag
    m) Syringe
    n) Paper towels
3) Open specimen bag and remove organ.
4) Place tourniquet at base of penis and cause moderate tumescence by injecting normal saline or water into corpora with small needle and syringe.
5) Using the scalpel, make a circumferential incision just underneath and around the glans.
6) Use the tweezers to lift up the skin of the penis and use the Kelly clamp to separate the skin from the Bucks Fascia by spreading the Kelly clamp. Repeat the procedure until the entire organ is degloved.
7) Use the small dissecting scissors to cut away the degloved skin.
8) Remove the tourniquet to and wipe away the saline with paper towels.
9) Insert the small tube/straw into the urethra in order to isolate the urethra. Make lateral incisions on either side of the tube/straw into the corpus spongiosum in order to cut out the urethra with the scalpel.
10) Using the scalpel, make two longitudinal incisions through the midline of each corpus cavernousum. Do not cut through the midline of the organ as you will go through the septum ad bypass the corpus cavernosum. You should notice a white layer of tissue, the tunica albuginea (TA) connected to the red spongy tissue, the corpus cavernosum (CC).
11) While gripping the white TA tissue with tweezers, use the dissecting scissors to separate the CC and TA. Circumvent the organ moving laterally from both longitudinal cuts until the septum is visible on both sides.
12) Use the dissecting scissors to cut through the fibrous septum and cut the isolated TA tissue away from the remainder of the organ. You should be left with a rectangular sheet of TA tissue.
13) Using the tweezers and L shaped dissecting scissors, clean off the TA by removing the remainder of the Buck's Fascia and CC that may remain.

14) Using the ruler, measure out 3 cm x 3 cm squares, making sure that the septum is in the middle of the square. Try and isolate the most dorsal region of the tissue. If the dissected TA is large enough, one dorsal and one proximal region can be cut.
15) Take the TA square(s) and wrap them in saline soaked gauze and put them in labeled bags. Place these bags into the fridge for the next day's testing.
16) All remaining biological waste should be placed into one large bag and put back into the freezer until proper disposal can be done. All tools and equipment should be cleaned based on biological protocols.

Specimen Preparation

1) Remove the previously isolated and dissected TA out of the fridge and place on petri dish.
2) Using a thickness measurement device (caliper or laser sensor), take 8 thickness measurements (two for each side of the square) of the tissue.
3) Add enough 1 X PBS solution to be able to completely immerse tissue. Allow up to 15 minutes to soak.
4) Repeat step 2.
5) Re-immerse tissue into PBS and add methylene blue dye to the container. Allow up to 15 minutes for dye to dissolve into tissue sample.
6) Using the premade clamps, place safety pin loops through the tissue in marked locations.
7) In the fume hood, use spray paint can and perforated metal sheet to speckle a pattern on the tissue sample. Speckles should be fine and dense, but separated with sufficient space.
8) Let paint dry on sample for 10 minutes.

Testing Apparatus

1) Biaxial:
   a) Ensure the biaxial is equipped with 50N load cells.
   b) Zero load cells
2) Camera system
   a) Set up tripod on the biaxial so that the camera focuses on the field of view.
   b) Set up light fixtures, making sure that they point down on the sample to prevent shadows in the images.
   c) Calibrate the DIC system with the rubber sample by loading the rubber sample on the biaxial and pull to about 0.2N in each direction. Adjust the brightness and focus.
   d) Calibrate the DIC system again with the calibration grid by taking approximately 30 images of the grid and running the images through the DIC software. These images allow the cameras to know where their field of view is in space and will ensure focus and aperture are sufficient for testing.
   e) Do not move or adjust the cameras after calibration.

Testing Protocol

1) Load the prepared sample onto the biaxial with the longitudinal direction along the A axis and pull to about 0.2N in each direction.
2) Capture an image of the sample and analyze the speckle pattern to ensure proper distribution. If not, remove the sample from the biaxial and re-speckle.
3) Fill the bath with 4 liters of 1 X PBS solution.
4) Slowly raise the bath to immerse the sample (quick immersion can cause speckles to fall off).
5) Repeat step 2.
6) Allow the sample to rest in the bath for about 15 minutes for the dye to dilute. After 15 minutes, slosh the water in the bath to dissipate it evenly through the solution.
7) Place the lid on the bath, making sure no air bubbles are trapped.
8) Precondition the sample by stretching the sample to 5% of the initial hooked length and unloading. Up to 50 cycles can be performed until the load peaks stabilize.
9) Immediately prior to beginning biaxial protocol, begin image capture at 2 images per second.
10) Biaxial protocol
    a) Pull the sample to 45N in both directions using displacement control of 0.1 mm per second.
    b) Hold the sample at the displacement of max load for 30 minutes.
    c) Slack the sample to 0.5N in both directions using displacement control of 0.1 mm per second.
11) Stop image collection.
12) Slack the sample manually to 0.1N and let it rest for 2 hours for recovery.
13) Repeat steps 9 and 10.
14) Remove the sample from the biaxial and wrap in saline soaked gauze and place in the freezer for future disposal with the remaining organ waste.
15) Drain water bath with vacuum and wipe bath dry with paper towels.
16) Remove crosshead screws of biaxial and to prevent salt buildup.

Data Analysis

1) Truncate the image sequence from the stress relaxation portion of the testing protocol by a factor of 10. Combine these images with the image sequence from the ramp up. Each sample
2) Run the combined images through the DIC software.
3) Correct the axes of the processed images by aligning the x axis with the longitudinal direction.
4) Export the data from the DIC and biaxial into excel sheets. Since these collected data at different frequencies, match up the data by trimming the rows.
5) Organize and combine the two data sheets together in a sheet with the following headings:
    a) Index: starting from 0
    b) exx[1] – Lagrange: from DIC
    c) eyy[1] – Lagrange: from DIC
    d) exy[1] – Lagrange: from DIC
    e) e1[1] – Lagrange: from DIC
    f) e2[1] – Lagrange: from DIC
    g) gamma[1] – Lagrange: from DIC
    h) A Deformation: A axis absolute displacement from biaxial

i) A Avg Load: A axis force reading from biaxial
j) B Deformation: B axis absolute displacement from biaxial
k) B Avg Load: B axis force reading from biaxial
l) A CSA: cross sectional area of sample
m) A Stress: A Avg Load divided by A CSA
n) B CSA: cross sectional area of sample
o) B Stress: B Avg Load divided by B CSA
p) A Deformation Shifted: A axis relative displacement from biaxial
q) B Deformation Shifted: B axis relative displacement from biaxial

6) Run the master excel sheet through the Matlab code in Appendix A.
7) To get the percent stress relaxation value, the stress at the peak load as well as the stress of the load 30 minutes after the peak was recorded.